AIP | The Journal of Chemical Physics

The behavior of active diffusiophoretic suspensions: An accelerated Laplacian dynamics study

Wen Yan and John F. Brady

Citation: The Journal of Chemical Physics **145**, 134902 (2016); doi: 10.1063/1.4963722
View online: http://dx.doi.org/10.1063/1.4963722
View Table of Contents: http://scitation.aip.org/content/aip/journal/jcp/145/13?ver=pdfcov
Published by the AIP Publishing

The behavior of active diffusiophoretic suspensions: An accelerated Laplacian dynamics study

Wen Yan[1,a)] and John F. Brady[2,b)]
[1]*Department of Mechanical and Civil Engineering, California Institute of Technology, Pasadena, California 91125, USA*
[2]*Divisions of Chemistry & Chemical Engineering and Engineering & Applied Science, California Institute of Technology, Pasadena, California 91125, USA*

(Received 1 July 2016; accepted 15 September 2016; published online 5 October 2016)

Diffusiophoresis is the process by which a colloidal particle moves in response to the concentration gradient of a chemical solute. Chemically active particles generate solute concentration gradients via surface chemical reactions which can result in their own motion — the self-diffusiophoresis of Janus particles — and in the motion of other nearby particles — normal down-gradient diffusiophoresis. The long-range nature of the concentration disturbance created by a reactive particle results in strong interactions among particles and can lead to the formation of clusters and even coexisting dense and dilute regions often seen in active matter systems. In this work, we present a general method to determine the many-particle solute concentration field allowing the dynamic simulation of the motion of thousands of reactive particles. With the simulation method, we first clarify and demonstrate the notion of "chemical screening," whereby the long-ranged interactions become exponentially screened, which is essential for otherwise diffusiophoretic suspensions would be unconditionally unstable. Simulations show that uniformly reactive particles, which do not self-propel, form loosely packed clusters but no coexistence is observed. The simulations also reveal that there is a stability threshold — when the "chemical fuel" concentration is low enough, thermal Brownian motion is able to overcome diffusiophoretic attraction. Janus particles that self-propel show coexistence, but, interestingly, the stability threshold for clustering is not affected by the self-motion. *Published by AIP Publishing.* [http://dx.doi.org/10.1063/1.4963722]

I. INTRODUCTION

Active diffusiophoretic suspensions refer to colloidal particles that are able to convert chemical energy to self-propulsion, usually through patterned surface reactivity.[1] Experimentally, such active particles exhibit very interesting behavior. Howse[2] showed that, at times long compared to the rotational Brownian motion time scale τ_R, the translational diffusivity of a single active particle is enhanced by $U_0^2\tau_R/6$, where U_0 is the self-propulsive active velocity. The collective behavior is even more intriguing. Active particles with attractive interactions were observed to exhibit dynamic clustering and phase separation in experiments by Theurkauff[3] and Palacci,[4] while particles with repulsive interaction show a transition between an uncorrelated motion and an ordered lattice.[5]

The Active Brownian Particle (ABP) model has been proposed to understand this phase behavior. In ABPs, the particle's self-propulsion velocity $\boldsymbol{U}_0 = U_0\boldsymbol{\xi}$, where U_0 is usually assumed to be a given constant and the particle's orientation, $\boldsymbol{\xi}$, is subject to rotational Brownian motion. The interactions between ABPs are typically assumed to be hard-particle collisions only (purely repulsive)[6] or a pairwise additive potential.[7] Under these circumstances, the interactions between ABPs are short-ranged and additive, and therefore, the collective behavior can be successfully explained by thermodynamic-type models, such as the ϕ^4 field theory,[8] density functional theory,[9] and motility-induced-phase-separation.[10,11] For example, the dilute-dense coexistence of active matter can be explained as a first-order gas-liquid phase transition with the introduction of swim pressure as the equation of state.[12,13]

However, the applicability of thermodynamic-type treatments of active diffusiophoretic suspensions is open to question when one considers the concentration field, c, of the chemical "fuel." For a single particle, Brady and Córdova-Figueroa[14,15] showed that a particle's motion can be determined by solving for the reactant solute concentration field $c(\boldsymbol{r})$ around the particle subject to a reaction boundary condition on the particle's surface. The propulsive, or swim, velocity now depends on the local value of the concentration: $U_0(c) \propto c$; particles swim faster with more "fuel" (cf. (1) below). When a second (or more) particle(s) is (are) present, this creates a disturbance to the concentration field, which affects the magnitude of swim velocity as the two (or more) particles compete for the fuel, but particle-particle attraction (or repulsion) can be induced via diffusiophoresis down the concentration gradient (∇c) caused by the other particle(s).

In fact, the self-propulsion and particle-particle interactions are not separable because they come from the same

a)Current address: Simons Center for Data Analysis, 160 Fifth Avenue, New York, New York 10010, USA. Electronic mail: wyan@simonsfoundation.org
b)jfbrady@caltech.edu

reactant concentration field $c(\boldsymbol{r})$. As we show below, the system behavior is controlled by the non-dimensional "fuel concentration" $S_D \sim c^E a^3$, where c^E is the *imposed* solute reactant concentration at infinity and a is the particle size. The parameter S_D can equivalently be thought of as the ratio of the reaction-induced velocity, U^{ph}, due to either swimming or down-gradient diffusiophoresis, to the Brownian velocity, U^B: $S_D \sim U^{ph}/U^B$, which is also a Péclet number: $S_D \sim U^{ph}a/D$, where D its Brownian diffusivity of the particles. For large S_D both the swimming ($\propto c$) and attraction ($\propto \nabla c$) are enhanced and so the system has more chance to form clusters by overcoming the randomizing translational Brownian motion.

The strength of the swim velocity and attractive interactions also depends on the Damköhler number $\mathrm{Da} = \kappa_0 a/D_R$, which is a measure of the rate of chemical reaction κ_0 to diffusion of the reactants D_R. Typical reactant solutes are much smaller than the reactive particles so that the diffusivity of reactant solutes $D_R \gg D$, and thus, the fuel concentration field is slaved to the location of the particles: $c(\boldsymbol{r}; \boldsymbol{X}(t))$, where $\boldsymbol{X}(t)$ is the instantaneous position(s) of the particle(s).

This "field-driven" nature of chemically active particles can result in system behavior that is fundamentally different from ABPs. To probe the system dynamics, the field c must be solved simultaneously with the particles' motion, and this must be done efficiently so that the collective motion of a large number of particles can be monitored. Because of their small size and rapid diffusion, the reactive solute concentration field is governed by Laplace's equation. For Laplace's equation, it is well known that a source or sink induces a long-range concentration disturbance similar to electrostatics: $c' \sim 1/r$, where r is the distance from the particle. However, the situation is more subtle for chemically active particles as the source or sink strength, which is the particle reactivity, is not fixed but depends on the local reactant concentration, which in turn depends on the presence of other reactive particles. We show explicitly in this work that the interaction between reactive particles is screened in a manner analogous to Brinkman[16,17] screening. Thus, one cannot simply impose a fixed $1/r$ interaction between particles as has been done in some simulation work.[4,18] Furthermore, although the interactions now take on an exponentially screened form, it is not correct to suppose that the interactions follow a pairwise Yukawa potential, because the screening can only be correctly accounted for *after* the solution of the full Laplace's equation governing the concentration field.

The purpose of this paper is to present an efficient computational algorithm for solving Laplace's equation for the concentration field surrounding a finite or infinite (periodic) number of chemically reactive particles and by doing so to determine the reaction-induced motion of the particles and examine the clustering phenomena displayed in these systems.

Solving Laplace's equation for N particles is never an easy task because it usually requires $O(N^2)$ or even $O(N^3)$ operations to apply the mesh-based finite difference or finite volume methods. Bonnecaze and Brady developed a method[19–21] to solve the many-body Laplace equation by a multipole scattering method. Their method achieves significant improvement by avoiding the use of a mesh, but still requires $O(N^2)$ or $O(N^3)$ explicit matrix construction and inversion. In this work we combine the method of Bonnecaze and Brady with Sierou's Accelerated Stokesian Dynamics (ASD),[22] achieving a matrix-free $O(N \log N)$ method.

We show that our Accelerated Laplacian Dynamics (ALD) can efficiently track the dynamics of chemically active diffusiophoretic systems. In Sec. II, we formulate the problem and present the solution methodology in Sec. III. In Sec. IV A 3, we clarify the concept of chemical screening with both analytical theory and via simulations. This also serves as a verification of our simulation method. Furthermore, chemical screening is essential for otherwise diffusiophoretic suspensions would be unconditionally unstable. Results for attractive sink and Janus particles in a periodic setting are reported in Sec. IV B. We analyze the simulation results to address two fundamental questions of chemically active diffusiophoretic suspensions: when does the clustering process start (the stability as a function of S_D) and when does it stop (what is the structure of the final state)?

II. PROBLEM FORMULATION

Small colloidal particles can move in response to a concentration gradient of a chemical solute. If the gradient is externally imposed, the process is referred to as diffusiophoresis; if the particle generates the gradient itself via, e.g., a surface chemical reaction it is called self-diffusiophoresis. Following the approach and notation of Brady,[15] (which has been shown to agree with more conventional approaches[23]), in both cases the velocity of a spherical colloidal particle of radius a can be written as

$$\boldsymbol{U} = -\frac{L(\Delta)}{6\pi\eta a} \oint \boldsymbol{n}\, k_B T c(\boldsymbol{x},t) dS, \tag{1}$$

where the nondimensional hydrodynamic mobility function $L(\Delta) = (3/2)\Delta^2(1 + \frac{2}{3}\Delta)/(1+\Delta)^3$, with $\Delta = \delta/a$, measures the flow of fluid with viscosity η in a layer of thickness δ adjacent to the colloidal particle where the particle-solute interactive force is operative, cf. Fig. 1. Here we have taken the simplest form of interactive force between the solute and the colloidal particle, namely, a hard-sphere repulsive force at a distance $r_c = a + \delta$ (and δ need not be small compared to the particle size a, although typically it is so). More general interactive forces will only have a quantitative effect; the work of Brady[15] details how to include these (and other) effects. Generalizations to nonspherical particles are also possible.[24]

The solute concentration enters the expression for the particle velocity multiplied by the thermal energy $k_B T$, which we recognize as the local osmotic pressure of the solute $\Pi(\boldsymbol{x},t) \equiv k_B T c(\boldsymbol{x},t)$. This permits the interpretation of the velocity as the result of a force balance between the Stokes drag of the solvent and the osmotic force of the solute: $\boldsymbol{F}^{drag} + \boldsymbol{F}^{osmo} = 0$, with $\boldsymbol{F}^{drag} = -6\pi\eta a \boldsymbol{U}$ and $\boldsymbol{F}^{osmo} = -L(\Delta) \oint \boldsymbol{n}\, k_B T c(\boldsymbol{x},t) dS$. That the osmotic force is a real, measurable, force can be appreciated by realizing that if one wanted to stop the colloidal particle from moving, say by

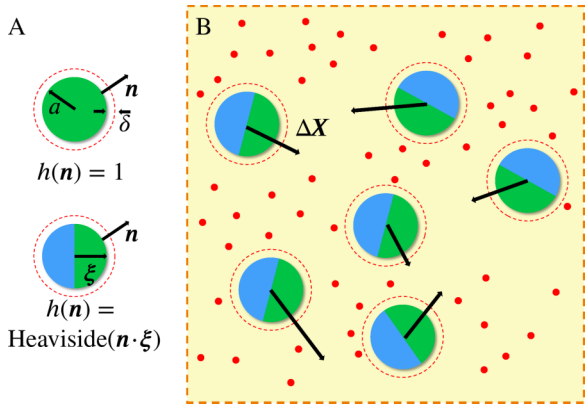

FIG. 1. (A) The uniformly reactive sink particle and the Janus particle with orientation vector $\boldsymbol{\xi}$. Both particles have radius a, interaction layer thickness δ, and surface normal vector $\boldsymbol{n}$. A reactive surface is colored green and a non-reactive surface is blue. Motion ($\Delta \boldsymbol{X}$) of each Janus particle in a system is governed by the over-damped Langevin equation (6). (B) The concentration field c of reactive solute molecules (shown by the red dots) is solved simultaneously with the motion of the active particles.

optical tweezers, then the force the tweezers would need to exert is precisely $\boldsymbol{F}^{osmo}$.

For chemically active particles, the catalytic reaction at the particle surface can be expressed as $R \rightarrow \theta P$, where R is the reactant, P is the product, and θ is the stoichiometry of the chemical reaction. In general, one needs the osmotic force arising from both the reactants and products, but, as shown by Córdova-Figueroa and Brady,[14] one only needs to scale (1) by the factor $(1 - \theta D_R/D_P)$, where D_R and D_P are the diffusivities of the reactants and products, respectively, to account for both reactants and products.

The reactant concentration satisfies the usual advection-diffusion equation

$$\frac{\partial c}{\partial t} + \nabla \cdot \boldsymbol{j}_R = 0, \tag{2}$$

where the reactant solute flux is given as

$$\boldsymbol{j}_R = \boldsymbol{u}c - D_R \nabla c, \tag{3}$$

and $\boldsymbol{u}$ is the velocity of the suspending fluid. In this study any fluid motion is the result of the motion of the colloidal particles, and thus, the relative importance of advection to diffusion is governed by the Péclet number $\mathrm{Pe} = Ua/D_R$. Typical phoretic or self-propulsive velocities are of order 1 μm/s for a micron-sized particle, while solute diffusivities are of order 10^3 μm^2/s so that the Péclet number is very small and fluid advection can be neglected. When particle-particle interaction is considered, the competition for "fuel" causes all particles slow down, and so $\mathrm{Pe} \ll 1$ remains valid. Similarly, the time scale to establish a steady solute concentration profile, a^2/D_R, is much faster than the time scale for the motion of the particle, either due to diffusiophoresis or to its intrinsic Brownian motion, so that the reactant/solute concentration distribution satisfies Laplace's equation

$$\nabla^2 c = 0. \tag{4}$$

We model the catalytic reaction at the particle surface as first order and, making use of the stochiometry/diffusivity factor $(1 - \theta D_R/D_P)$, the reaction can be taken to be irreversible,

$$\boldsymbol{n} \cdot \boldsymbol{j}_R = -\kappa_0 h(\boldsymbol{n}) c, \tag{5}$$

where κ_0 is the surface reaction rate constant (units of *length*/*time*) and the nondimensional function $h(\boldsymbol{n})$ describes the patterned reactivity on the particle surface whose outer normal is $\boldsymbol{n}$. For uniformly reactive particles $h(\boldsymbol{n}) = 1$, while a particle with $h(\boldsymbol{n}) = \mathrm{Heaviside}(\boldsymbol{n} \cdot \boldsymbol{\xi})$ describes the pattern of a Janus particle with orientation vector $\boldsymbol{\xi}$: $h = 1$ on the reactive hemisphere and $h = 0$ on the passive hemisphere, see Fig. 1. Particles for which $(1 - \theta D_R/D_P) > 0$ reduce the concentration of reactant near their surface and will attract a second particle by diffusiophoresis; such particles act as chemical sinks; those with $(1 - \theta D_R/D_P) < 0$ act as sources.

The diffusiophoretic system shares many similarities with electrostatics: both are governed by Laplace's equation with the reactant concentration being the analog of the electrostatic potential, and chemical sink/source particles are analogous to negative/positive charges, etc. There is, however, an important difference. In an electrostatic system, the electric field does not disappear if charges are not destroyed. In a diffusiophoretic system, on the other hand, the concentration of reactant is subject to chemical reaction, and when all the reactants (or fuel) are consumed by the particles, the concentration goes to zero and all motion (apart from the particles' intrinsic Brownian motion) ceases. Thus, to achieve a steady state with reactive particles, we need to supply reactant (and remove product) at the same rate at which it is consumed (produced) by the particles. In experiments with a monolayer of active particles,[3] reactant is provided by diffusion from a reservoir above the monolayer.

In this work, we shall consider two types of systems: finite and periodic. For finite systems, we have a finite number of particles moving in an infinite bath of solute (reactant and product), and we specify a boundary condition of a constant reactant concentration c^∞ as the distance goes to infinity. Physically, reactant diffuses from infinity to the particle region to compensate for the consumption by the active particles; no other reactant sources are needed. For a periodic system there is no "infinity," and the condition to have a steady state is for a homogeneous generation of reactant at a rate $\langle s \rangle$ that balances the rate of consumption so that the volume average solute concentration $\langle c \rangle$ is a spatial (unit cell average) constant. This makes the system as a whole "chemically neutral" — the positive uniform chemical source balances the negative reactive sink particles — and ensures that the long-range interactions typical in Laplace systems are convergent. The uniform source of reactant is the counterpart of the constant negative "electrostatically neutralizing background" in a one component plasma (OCP). Also, similar (but not identical) to electrostatic systems, diffusiophoretic interactions are screened — a phenomenon known as Brinkman screening,[17] which we discuss in Sec. IV.

The problem is now the following: for a system of active particles at locations $\boldsymbol{X}(t)$, we need to solve for the reactant concentration field governed by the steady Laplace's equation

(4) at all field points $\boldsymbol{r}$ outside the particles subject to a first order surface reaction boundary condition (5) for either (or both) uniform reactive particles ($h(\boldsymbol{n}) = 1$) or (and) Janus particles ($h(\boldsymbol{n}) = \text{Heaviside}(\boldsymbol{n} \cdot \boldsymbol{\xi})$) for either a finite number of active particles or in infinite periodic system. From the solution for $c(\boldsymbol{r}; \boldsymbol{X}(t))$, we determine the phoretic velocity $\boldsymbol{U}$ of an active particle from (1) for a given interactive length $\Delta = \delta/a$ and a stoichiometry/diffusivity factor $(1 - \theta D_R/D_P)$. The active particles are then advanced to a new location from the overdamped Langevin equation incorporating Brownian translation (and rotation in the case of Janus particles),

$$\Delta \boldsymbol{X} = \boldsymbol{U}\Delta t + \Delta \boldsymbol{X}^B + \Delta \boldsymbol{X}^P, \tag{6}$$

where the Brownian displacement has zero mean, $\overline{\Delta \boldsymbol{X}^B} = 0$ and covariance, $\overline{\Delta \boldsymbol{X}^B \Delta \boldsymbol{X}^B} = 2D\Delta t$, where $D = k_B T/6\pi\eta a$ is the translation Brownian diffusivity of an active particle. A hard-sphere displacement $\Delta \boldsymbol{X}^P$ is implemented to prevent particles from overlapping determined from a potential-free algorithm.[25,26] Once the active particles have been advanced to their new location, a new concentration field $c(\boldsymbol{r}; \boldsymbol{X}(t))$ must be found and the process repeated until a steady state is reached. For Janus particles, rotational Brownian motion ($D_{rot} = k_B T/8\pi\eta a^3$) is included as a diffusive reorientation event at each time step and calculated with the unbiased move method.[27] Equation (6) employs a simple Euler scheme for clarity; higher order schemes such as fifth order Adams-Bashforth multi-step scheme are also used in simulation.

In writing the displacements (6) we have neglected any hydrodynamic interactions (HI) among the active particles. HI can be included by combining the method developed in this paper with Stokesian dynamics[22] for hydrodynamically interacting colloidal particles. It should be noted that the hydrodynamic flow field created by a phoretic particle typically corresponds to a force quadrupole with a velocity field decaying as $1/r^3$ or, for Janus particles, as a force dipole or stresslet, decaying as $1/r^2$.

III. METHOD FOR SOLUTION OF LAPLACE'S EQUATION

The disturbance to the concentration field caused by a single reactive particle decays as q/r, where q is the net reactant consumption rate, which is the counterpart of the electrostatic charge q_e. Despite the simple form of the potential disturbance, the difficulty of solving the Laplace problem for a system of interacting particles is three-fold.

First, the particles have finite size and the concentration or potential field has a distribution on the surface of a particle; thus, the perturbed concentration field induced by an active particle must be considered to a higher order than simply a point sink or source. Second, the $1/r$ interaction is long-ranged and must be properly summed for both finite and periodic systems. Third, to solve for the collective dynamics, the motion of hundreds or thousands of particles must be followed, which requires a highly efficient solution methodology.

The strategy adopted here is to split the problem into three parts. First, we follow the approach of Bonnecaze and Brady[19] and represent the field induced by each particle by a multipole expansion, including the monopole q (scalar), dipole $\boldsymbol{S}$ (vector), and quadrupole $\boldsymbol{Q}$ (second order tensor), defined as

$$q_\beta = \int_{S_\beta} \boldsymbol{j}_R \cdot \boldsymbol{n}\, dS, \tag{7}$$

$$\boldsymbol{S}_\beta = \int_{S_\beta} (\boldsymbol{x}\boldsymbol{j}_R + D_R c \boldsymbol{I}) \cdot \boldsymbol{n}\, dS, \tag{8}$$

$$\boldsymbol{Q}_\beta = \int_{S_\beta} \Big(\big[\boldsymbol{x}\boldsymbol{x} - \tfrac{1}{3}(\boldsymbol{x}\cdot\boldsymbol{x})\boldsymbol{I}\big]\boldsymbol{j}_R \cdot \boldsymbol{n} + \big[\boldsymbol{x}\boldsymbol{n} + \boldsymbol{n}\boldsymbol{x} - \tfrac{2}{3}(\boldsymbol{n}\cdot\boldsymbol{x})\boldsymbol{I}\big] D_R c \Big) dS, \tag{9}$$

where S_β is the surface of particle β, $\boldsymbol{x}$ is a vector pointing from the particle center to its surface, and $\boldsymbol{I}$ is the identity tensor. The quadrupole $\boldsymbol{Q}_\beta$ is defined to have zero trace. The definition of the multipoles here mathematically originates from Green's third identity, which gives the value of a harmonic function in a domain by an integral of its value, gradient, and Green's function on the boundary of the domain. In this work, the space between particles is the domain and particle surfaces are the boundary of the domain. More details related to this method can be found in the work by O'Brien.[28]

Each particle β creates a disturbance concentration field that takes the form,

$$\begin{aligned} c'(\boldsymbol{r}) &= c(\boldsymbol{r}) - c^E(\boldsymbol{r}) \\ &= \frac{1}{4\pi D_R}\left(\frac{q_\beta}{|\boldsymbol{r} - \boldsymbol{r}_\beta|} + \boldsymbol{S}_\beta \cdot \nabla_\beta \frac{1}{|\boldsymbol{r} - \boldsymbol{r}_\beta|} + \frac{1}{2}\boldsymbol{Q}_\beta : \nabla_\beta \nabla_\beta \frac{1}{|\boldsymbol{r} - \boldsymbol{r}_\beta|} + \cdots \right), \end{aligned} \tag{10}$$

where $\boldsymbol{r}$ is the field point, $\boldsymbol{r}_\beta$ is the center of particle β, and $\nabla_\beta = \partial/\partial \boldsymbol{r}_\beta$. The gradients ∇c and $\nabla\nabla c$ can also be constructed in the same fashion. In (10), c^E refers to the externally imposed concentration that is either c^∞ in the case of a finite system or the average $\langle c \rangle$ in the case of a periodic system. The expansion (10) follows directly from the integral representation for the solution to Laplace's equation and is the same as one would do for the electrostatic potential with the exception that the source strengths, q_β, $\boldsymbol{S}_\beta$ and $\boldsymbol{Q}_\beta$, are not given but must be found as a solution to the many-body Laplace problem. (Note that the finite volume of a particle has been included in the definition of the multipoles, and thus, Equation (10) takes a form as if all multipoles act at the particle center.) Although truncated at this level, the multipole description preserves all the important aspects of the problem and also proves to be accurate even when particles are close to one another.

Next, we need to determine the source strengths of a particle in response to the concentration field in which it finds itself. This can be accomplished by so-called Faxen laws, which relate the multipoles $q_\alpha, \boldsymbol{S}_\alpha, \boldsymbol{Q}_\alpha$ of particle α to the concentration field $c(\boldsymbol{r}_\alpha) = c^E + c'$, where $c'(\boldsymbol{r}_\alpha)$ is the disturbance field caused by all the other particles β. Faxen laws follow from the reciprocal theorem for Laplace's equation and allow one to by-pass the detailed solution for the concentration field and proceed directly to the moment strengths. Because

the reaction boundary condition at a particle surface is first order and linear, the Faxen laws take a linear form,

$$\begin{pmatrix} q_\alpha \\ \boldsymbol{S}_\alpha \\ \boldsymbol{Q}_\alpha \end{pmatrix} = \boldsymbol{C} \cdot \begin{pmatrix} c(\boldsymbol{r}_\alpha) \\ \nabla c(\boldsymbol{r}_\alpha) \\ \nabla\nabla c(\boldsymbol{r}_\alpha) \end{pmatrix}, \tag{11}$$

where the concentration field c is evaluated at the center of particle α and originates from each particle β as given by (10). The matrix $\boldsymbol{C}$ is the analog of the "capacitance matrix" for electrostatics.

A. Faxen laws for reactive particles

For a uniform reactive particle, $h(\boldsymbol{n}) = 1$, the Faxen laws take a rather simple block diagonal form resulting from the particle's symmetry,

$$q_\alpha = -\frac{\mathrm{Da}}{1+\mathrm{Da}} 4\pi a\, D_R\, c(\boldsymbol{r}_\alpha), \tag{12}$$

$$\boldsymbol{S}_\alpha = -\frac{\mathrm{Da}-1}{\mathrm{Da}+2} 4\pi a^3 D_R \nabla c(\boldsymbol{r}_\alpha), \tag{13}$$

$$\boldsymbol{Q}_\alpha = -\frac{\mathrm{Da}-2}{3\mathrm{Da}+9} 4\pi a^5 D_R \nabla\nabla c(\boldsymbol{r}_\alpha), \tag{14}$$

where the Damköhler number $\mathrm{Da} = \kappa_0 a/D_R$ measures the rate of the chemical reaction to diffusion of the reactant. The derivation of the Faxen laws is given in Appendix A. For slow reaction rates or small Damköhler number, the sink strength q_α is linear in Da, while the dipole and quadrupole remain finite. At the other extreme of fast reactions, all multipoles are finite as $\mathrm{Da} \to \infty$. The concentration field $c(\boldsymbol{r}_\alpha)$ (which is due to all particles other than α) and its gradients are evaluated at the center of particle α.

It is important to note that even though the dipole and quadrupole do not vanish as $\mathrm{Da} \to 0$, since there is no macroscopically imposed concentration gradient, when the reaction rate goes to zero, the monopole of each particle vanishes and there are no gradients induced by the particles. As $\mathrm{Da} \to 0$ the concentration becomes uniform everywhere and all reaction-induced motion ceases.

For Janus particles, $h(\boldsymbol{n}) = \mathrm{Heaviside}(\boldsymbol{n}\cdot\boldsymbol{\xi})$, and in this case the Faxen law matrix $\boldsymbol{C}$ is not diagonal. The asymmetric surface reaction requires all multipoles even when the concentration field is a constant. The relation cannot be expressed in closed analytical form because all multipole moments recursively relate to each other. We use the Boundary Element Method (BEM) to numerically solve for the Faxen laws. The single particle response is truncated at dipole level for simplicity,

$$\begin{pmatrix} q_\alpha \\ \boldsymbol{S}_\alpha \end{pmatrix} = \boldsymbol{C}(\mathrm{Da}, \boldsymbol{\xi}_\alpha) \cdot \begin{pmatrix} c(\boldsymbol{r}_\alpha) \\ \nabla c(\boldsymbol{r}_\alpha) \end{pmatrix}. \tag{15}$$

Here the matrix is not only a function of Da as it was for the uniform reaction case, but is also dependent on the particle orientation vector $\boldsymbol{\xi}$ due to the asymmetry of a Janus particle. The BEM formulation and the detailed matrix entries can be found in Appendix B. For a single particle, the solution given by $\boldsymbol{C}$ at the dipole level matches previous work very well.[14] The asymptotic dependence of $\boldsymbol{C}(\mathrm{Da}, \boldsymbol{\xi})$ for small and large Da is the same as for the uniform reactive particle.

In addition to the Faxen laws for the sink and dipole strength, for the particle dynamics we need the phoretic velocity of an active particle given by (1), which is proportional the integral

$$\boldsymbol{B}_\alpha = \int_{S_\alpha} \boldsymbol{n} c\, dS. \tag{16}$$

For the uniform reaction case $\boldsymbol{B}$ is simply related to the dipole moment $\boldsymbol{S}$,

$$\boldsymbol{B}_\alpha = \frac{1}{D_R}\left(\frac{1}{1-\mathrm{Da}}\right)\boldsymbol{S}_\alpha = \frac{1}{2+\mathrm{Da}} 4\pi a^3 \nabla c(\boldsymbol{r}_\alpha), \tag{17}$$

showing that there is no self-motion for a homogeneous reactive particle; reaction-induced motion arises from the concentration gradient created by the other particles, corresponding to normal diffusiophoresis.

Note that from (1) the particle velocity is proportional to $-\boldsymbol{B}_\alpha$ so that the phoretic particle moves down the concentration gradient of solute or reactant and that gradient is provided by the other active particles. The motion is down the concentration gradient because we have assumed repulsive interactions between the solute and the particle at the length δ; attractive interactions would give motion in the opposite direction. And, in general, it is possible to have a mixture of repulsive and attractive phoretic particles. We consider only repulsive particles in this work. It is a simple matter to extend the method presented here to attractive particles or to mixtures of repulsive and attractive particles.

For a Janus particle there is net motion both due to the nonuniform reaction on the particle surface, i.e., proportional to $c(\boldsymbol{r}_\alpha)$, and due to the phoretic motion down a concentration gradient. Thus, $\boldsymbol{B}_\alpha$ takes the form

$$\boldsymbol{B}_\alpha = \boldsymbol{M}_B(\mathrm{Da}, \boldsymbol{\xi}) \cdot \begin{pmatrix} c(\boldsymbol{r}_\alpha) \\ \nabla c(\boldsymbol{r}_\alpha) \end{pmatrix}. \tag{18}$$

The phoretic mobility matrix $\boldsymbol{M}_B$ is related to $\boldsymbol{C}$ and is given in Appendix B.

B. The concentration disturbance from other particles: Finite and periodic systems

One can find particle α's multipoles, q_α, $\boldsymbol{S}_\alpha$, and $\boldsymbol{Q}_\alpha$, from its response to other particles $\beta \neq \alpha$, each of which creates the disturbance (10) at α's center $\boldsymbol{r}_\alpha$. In this subsection, we describe how to formulate and compute the disturbance field for both finite and periodic systems. In a finite system, the external field $c^E = c^\infty = \text{const.}$ is specified as the boundary condition at infinity. Despite the long-range nature of particle disturbances, no convergence problem arises because the sum is over a finite number of particles and no cutoff is necessary nor employed. For N particles the many-body concentration disturbances can be written in the matrix form,

$$\begin{pmatrix} \boldsymbol{c}' \\ \nabla \boldsymbol{c}' \\ \nabla\nabla \boldsymbol{c}' \end{pmatrix} = \mathcal{E} \cdot \begin{pmatrix} \boldsymbol{q} \\ \boldsymbol{S} \\ \boldsymbol{Q} \end{pmatrix}, \tag{19}$$

where $\boldsymbol{q}$ is now a vector of sink strengths $\boldsymbol{q} = \{q_1, q_2, \ldots, q_N\}$, as is the concentration disturbance $\boldsymbol{c}' = \{c'(\boldsymbol{r}_1),$

$c'(\boldsymbol{r}_2),\ldots,c'(\boldsymbol{r}_n)\}$, and similarly for the dipole and quadrupole. The $(11N\times 11N)$ matrix $\mathcal{E}$ is the counterpart to the "potential matrix" in many-body electrostatic problems.[19] The entries in $\mathcal{E}$ follow directly from (10), and note that the self-terms in $\mathcal{E}$ are zero because the matrix sums over all particles $\beta\neq\alpha$ for each particle α.

In a periodic system $c(\boldsymbol{r})=c^E(\boldsymbol{r})+c'(\boldsymbol{r})$ still holds, but there is no boundary condition at infinity. Rather, $c^E=\langle c\rangle$, the volumetric average in the unit cell, as discussed in Sec. II. In general, $\langle c\rangle$ can consist of a constant plus a term linear in $\boldsymbol{r}$, i.e., $\boldsymbol{G}\cdot\boldsymbol{r}$, where $\boldsymbol{G}$ is a constant gradient. The gradient term is necessary when determining, e.g., the effective conductivity of a distribution of particle inclusions as done by Bonnecaze and Brady.[20] Here, we do not impose any macroscopic concentration gradient and shall take $\langle c\rangle$ to be a constant. (Note, there are *microscopic* concentration gradients induced by the active particles.)

For the periodic case, the linear relation (19) remains valid, but the explicit construction of the matrix elements is not as straightforward as one now has a periodic sum of long-range multipole interactions, which are computed using the Ewald summation technique. The convergence of the Ewald sum is guaranteed by the homogeneously distributed source $\langle s\rangle$ that provides the "chemically neutralizing background." Physically, the distributed source must be included in the system for otherwise the reactant concentration field governed by Laplace's equation would be $c=0$ everywhere — the only periodic solution possible would be the consumption of all reactants.

Bonnecaze and Brady[19] have a thorough discussion of the Ewald sum and the convergence in the presence of distributed sources and their approach can be used here with only a slight modification. In the work of Bonnecaze and Brady,[19] the neutralizing source was distributed uniformly throughout both the fluid and the particles. Here, however, the source is only in the fluid phase V_f and contributes to the concentration at a point an amount proportional to $\int_{V_f}(\langle s\rangle/r)\,dV$, which can be rewritten as an integral over all space minus the value within the particles: $\int_{V_f}(\langle s\rangle/r)\,dV=\int_V(\langle s\rangle/r)\,dV-\sum_\beta\int_{V_\beta}(\langle s\rangle/r)\,dV$. Thus, the "charge" of each particle β can be replaced with an effective charge $q_\beta^{eff}=q_\beta-V_\beta\langle s\rangle$, where V_β is the volume of particle β. One can now follow the work of Bonnecaze and Brady[19] where it was shown that the concentration field at any point in the fluid (outside the particles) can be written without approximation as

$$c(\boldsymbol{r})-\langle c\rangle=\frac{a^2\langle s\rangle}{2D_R}+\frac{1}{4\pi D_R}\sum_\beta\left(\frac{q_\beta^{eff}}{|\boldsymbol{r}-\boldsymbol{r}_\beta|}+\boldsymbol{S}_\beta\cdot\nabla_\beta\frac{1}{|\boldsymbol{r}-\boldsymbol{r}_\beta|}+\frac{1}{2}\boldsymbol{Q}_\beta:\nabla_\beta\nabla_\beta\frac{1}{|\boldsymbol{r}-\boldsymbol{r}_\beta|}+\cdots\right)$$
$$-\frac{1}{4\pi D_R}\int_V\left(\frac{\langle s\rangle}{|\boldsymbol{r}-\boldsymbol{r}'|}+n\langle\boldsymbol{S}\rangle\cdot\nabla'\frac{1}{|\boldsymbol{r}-\boldsymbol{r}'|}+n\frac{1}{2}\langle\boldsymbol{Q}\rangle:\nabla'\nabla'\frac{1}{|\boldsymbol{r}-\boldsymbol{r}'|}\right)dV'. \tag{20}$$

And, the condition of chemical neutrality relates the average effective charge to the uniform source,

$$n\langle q^{eff}\rangle=\langle s\rangle=n\langle q\rangle/(1+\phi), \tag{21}$$

and particle β's effective charge is

$$q_\beta^{eff}=q_\beta+\phi\langle q\rangle/(1-\phi), \tag{22}$$

where n is the number density of particles and $\phi=4\pi a^3n/3$ their volume fraction (all particles have been taken to have the same volume).

Equation (20) is an absolutely convergent expression for the concentration field for any distribution — periodic or random — of reactive particles. A check on the correctness of this can be seen by ensemble averaging the concentration at $\boldsymbol{r}$ over all possible realizations of the reactive particles β. The discrete sum $\sum_\beta q_\beta^{eff}\Rightarrow\int n\langle q^{eff}\rangle$ showing that the sum and the "backflow" integral over $\langle s\rangle$ cancel, as do the dipole and quadrupole terms. In addition, because the particles are excluded from being any closer to the field point $\boldsymbol{r}$ than their radii a and thus there is a contribution from the uniform source in the excluded region from 0 to a: $-(1/4\pi D_R)\int_0^a\langle s\rangle/(|\boldsymbol{r}-\boldsymbol{r}'|)dV'=-a^2\langle s\rangle/2D_R$, which precisely cancels the constant source term in (20). (The dipole and quadrupole contributions from this excluded volume region are zero.)

We now use this convergent formulation for simulation with periodic boundary conditions. Both the particle positions and the concentration field are periodic, and we consider a periodic cubic cell defined by cell vectors $(\boldsymbol{a}_1,\boldsymbol{a}_2,\boldsymbol{a}_3)$ with N particles $(\boldsymbol{r}_1,\boldsymbol{r}_2,\ldots,\boldsymbol{r}_N)$ in the primitive cell. The cell volume $V_0=(\boldsymbol{a}_1\times\boldsymbol{a}_2)\cdot\boldsymbol{a}_3=a_1a_2a_3$. On the unit cell the Fourier expansion follows the convention,

$$f(\boldsymbol{x})=\sum_{\boldsymbol{k}}\hat{f}(\boldsymbol{k})e^{-2\pi i\boldsymbol{k}\cdot\boldsymbol{x}},$$
$$\hat{f}(\boldsymbol{k})=\frac{1}{V_0}\int_{\text{cell}}f(\boldsymbol{x})e^{2\pi i\boldsymbol{k}\cdot\boldsymbol{x}}d\boldsymbol{x}. \tag{23}$$

To calculate the periodic sum efficiently, the Ewald summation technique is used.[29,30] For $\boldsymbol{r}\neq\boldsymbol{r}_\beta$, i.e., for any spatial point not on a particle position, we write

$$c(\boldsymbol{r})=\langle c\rangle+c'_{real}(\boldsymbol{r})+c'_{wave}(\boldsymbol{r}), \tag{24}$$

where

$$c'_{real}(\boldsymbol{r}) = \frac{1}{4\pi D_R}\sum_{\beta} q_{\beta}^{eff}\frac{\mathrm{Erfc}(\sqrt{\pi/\zeta}|\boldsymbol{r}-\boldsymbol{r}_{\beta}|)}{|\boldsymbol{r}-\boldsymbol{r}_{\beta}|}, \tag{25}$$

$$c'_{wave}(\boldsymbol{r}) = \frac{1}{4\pi D_R V_0}\sum_{\boldsymbol{k}\neq 0}\sum_{\beta} q_{\beta}^{eff} e^{2\pi i\boldsymbol{k}\cdot\boldsymbol{r}_{\beta}}\frac{e^{-\zeta\pi k^2}}{\pi k^2}e^{-2\pi i\boldsymbol{k}\cdot\boldsymbol{r}}. \tag{26}$$

Here ζ is the splitting parameter that controls the rate of convergence of real- and wave-space sums; the optimal choice of ζ has been thoroughly discussed.[30] We have only written the "charge" terms in (25) and (26) to illustrate the procedure. The dipole and quadrupole terms can be found in Appendix C or in the work of Bonnecaze and Brady.[19] Note that the removal of the $\boldsymbol{k} = 0$ term in the wave-space sum follows directly from the "backflow" integral over the uniform source distribution $\langle s\rangle$ in (20).

Equations (25) and (26), when added together, give the solution $c(\boldsymbol{r})$ for any spatial point. From the definition of $\mathcal{E}$ in (19) and the formulation of Faxen laws, we need the field that any particular particle responds to, *excluding* the contribution from the particle α itself, and the field is be evaluated at the particle's center $\boldsymbol{r}_{\alpha}$. Thus, an additional "self-correction" must be added to the sum.

The necessity of a self-term can also be appreciated by an analogy to the energy calculation in an electrostatic system. In that case, it is well known that the energy contribution from each charge q_i is $q_i\phi_{[i]}/2$, where $\phi_{[i]}$ is the electrostatic potential at the location of q_i excluding the contribution from the charge q_i itself. Therefore, the contribution from particle α must be removed from the Ewald sum. For example, relating q to c' the self-term is $-q_{\alpha}^{eff}/2\pi D_R\sqrt{\zeta}$.

To complete the calculation, we need all the elements of the potential matrix $\mathcal{E}$,

$$\mathcal{E} = \begin{pmatrix} \boldsymbol{E}_{cq} & \boldsymbol{E}_{\nabla q} & \boldsymbol{E}_{\nabla\nabla q} \\ \boldsymbol{E}_{cS} & \boldsymbol{E}_{\nabla\nabla S} & \boldsymbol{E}_{\nabla\nabla S} \\ \boldsymbol{E}_{cQ} & \boldsymbol{E}_{\nabla\nabla Q} & \boldsymbol{E}_{\nabla\nabla Q} \end{pmatrix}. \tag{27}$$

Equations (25) and (26), with the self-term $-q_{\alpha}^{eff}/2\pi D_R\sqrt{\zeta}$, give the contribution $\boldsymbol{E}_{cq}$. The other terms can be found in Appendix C.

C. Problem closure: Iterative solver

Combining all particles' response to their environment via the Faxen laws (11), we can form a "grand capacitance" matrix C,

$$\begin{pmatrix} \boldsymbol{q} \\ \boldsymbol{S} \\ \boldsymbol{Q} \end{pmatrix} = C\cdot\left[\begin{pmatrix} c^E \\ \nabla c^E \\ \nabla\nabla c^E \end{pmatrix} + \begin{pmatrix} c' \\ \nabla c' \\ \nabla\nabla c' \end{pmatrix}\right], \tag{28}$$

where C depends on the Damköhler number and, in the Janus case, the particle orientation vector $\boldsymbol{\xi}$. Combining (28) with (19), we have

$$(\boldsymbol{I} - C\cdot\mathcal{E})\cdot\begin{pmatrix} \boldsymbol{q} \\ \boldsymbol{S} \\ \boldsymbol{Q} \end{pmatrix} = C\cdot\begin{pmatrix} c^E \\ \nabla c^E \\ \nabla\nabla c^E \end{pmatrix}. \tag{29}$$

For a given configuration of particles, C and $\mathcal{E}$ are known, as is the "imposed" concentration field c^E.

A standard GMRES (Generalized minimal residual method) iterative solver can be applied to solve for the unknown multipole moments $\boldsymbol{q}$, $\boldsymbol{S}$, and $\boldsymbol{Q}$. In GMRES, the linear system $\boldsymbol{Ax} = \boldsymbol{b}$ is solved in such a way that $\boldsymbol{A}$ appears only as an operator; the operator returns a new vector $\boldsymbol{Ax}$ for any given vector $\boldsymbol{x}$. Such an operator nature allows us to employ iteration without explicitly building the matrix $\boldsymbol{A}$. Here, $\boldsymbol{A} = (\boldsymbol{I} - C\cdot\mathcal{E})$, $\boldsymbol{x} = (\boldsymbol{q},\boldsymbol{S},\boldsymbol{Q})$, and $\boldsymbol{b} = C\cdot(c^E,\nabla c^E,\nabla\nabla c^E)$.

After the iterative solver converges, the solution vector $(\boldsymbol{q},\boldsymbol{S},\boldsymbol{Q})$ for each particle is known and, from the single particle capacitance matrices $\boldsymbol{C}$ and mobility matrices $\boldsymbol{M}_B$, the osmotic driving force on each particle is

$$\boldsymbol{F}_{\beta}^{osmo} = -k_BTL(\Delta)\boldsymbol{M}_B\cdot\boldsymbol{C}^{-1}\cdot\begin{pmatrix} q_{\beta} \\ \boldsymbol{S}_{\beta} \\ \boldsymbol{Q}_{\beta} \end{pmatrix}. \tag{30}$$

Computational cost for computing $\boldsymbol{F}_{\beta}^{osmo}$ is negligible compared with that for computing the moments. The inversion of $\boldsymbol{C}$ requires $O(11^3)$ (or only 4^3 at the dipole level), and thus computing $\boldsymbol{F}^{osmo}$ requires $N\times O(11^3)$ operations, not $O((11N)^3)$ operations.

D. Matrix-free implementation

Computationally, C is diagonal for homogeneously reactive particles and block diagonal in the Janus case and only requires $O(N)$ operations. However, $\mathcal{E}$ is dense because of the long-range nature of Laplace's equation. Explicit construction and storage of the matrix $\mathcal{E}$ requires a large amount of memory and slow operations ($O(N^2)$ matrix-vector multiplication). Therefore, the key step to achieving an efficient solver is to eliminate the explicit large matrix operations. Below we briefly describe the implementation utilizing the matrix-free operator nature of a GMRES solver.

For a finite number of particles with an imposed concentration field, the strategy is straightforward: $(c'(\boldsymbol{r}_{\alpha}),\nabla c'(\boldsymbol{r}_{\alpha}),\nabla\nabla c'(\boldsymbol{r}_{\alpha}))$ for each particle α in (19) is directly summed with the tile algorithm used in the self-gravitating N-body problem utilizing GPU shared memory.[31] Compared to explicitly building and storing the matrix C with the CPU (3.1 GHz 2nd-gen Intel Core i), the GPU (nVidia GTX 580 & GTX 680, Fermi and Kepler architecture) method used here is able to achieve 100×speedup and uses about 1% of memory.

For the periodic case of Equation (19), which includes Ewald summation, the calculations are done on the GPU via the Particle Mesh Ewald (PME hereafter) method.[30] Successful PME relies on the choice of the splitting parameter ζ such that the real-space sum is convergent within several neighboring particles' contributions. Thus, the real-space sum is reduced from a dense matrix-vector multiplication to a sparse one. GPU performs well in such situations.

The wave-space sum is efficiently calculated with Fast Fourier Transforms (FFTs) in PME.[32] For future compatibility to include hydrodynamics, we follow the PME convention of accelerated Stokesian dynamics of Sierou and Brady,[22] which uses $5\times5\times5$ mesh and $5\times5\times5$ Lagrangian interpolation for each particle by ensuring for each particle β,

$$\sum_m q_m e^{2\pi i\boldsymbol{k}\cdot(\boldsymbol{r}_m-\boldsymbol{r})} = q_\beta^{eff} e^{2\pi i\boldsymbol{k}\cdot(\boldsymbol{r}_\beta-\boldsymbol{r})}, \tag{31}$$

$$\sum_m q_m e^{2\pi i\boldsymbol{k}\cdot(\boldsymbol{r}_m-\boldsymbol{r})} = 2\pi i\boldsymbol{S}_\beta\cdot\boldsymbol{k} e^{2\pi i\boldsymbol{k}\cdot(\boldsymbol{r}_\beta-\boldsymbol{r})}, \tag{32}$$

$$\sum_m q_m e^{2\pi i\boldsymbol{k}\cdot(\boldsymbol{r}_m-\boldsymbol{r})} = -2\pi^2\boldsymbol{Q}_\beta:\boldsymbol{k}\boldsymbol{k} e^{2\pi i\boldsymbol{k}\cdot(\boldsymbol{r}_\beta-\boldsymbol{r})}, \tag{33}$$

where m refers to point charges on the mesh points. The full Ewald sum given in (C2), including all $q_\beta^{eff}, \boldsymbol{S}_\beta, \boldsymbol{Q}_\beta$, and $\boldsymbol{r}_\beta$ terms, is now equal to and can be replaced by a sum of q_m terms on a regular mesh filling the entire periodic simulation box,

$$c'_{wave}(\boldsymbol{r}) = \frac{1}{4\pi D_R V_0}\sum_{\boldsymbol{k}\neq0}\sum_m q_m e^{2\pi i\boldsymbol{k}\cdot\boldsymbol{r}_m}\frac{e^{-\zeta\pi k^2}}{\pi k^2}e^{-2\pi i\boldsymbol{k}\cdot\boldsymbol{r}}, \tag{34}$$

which can be efficiently summed by 3D-FFT with $O(M\log M)$ operations for M mesh points. The $\nabla c'_{wave}(\boldsymbol{r})$ and $\nabla\nabla c'_{wave}(\boldsymbol{r})$ terms can be written in the same fashion with an extra $2\pi\boldsymbol{k}$ factor and can also be calculated by 3D-FFT. GPU is also used to achieve better performance.

IV. RESULTS

We demonstrate the methodology and the physics of chemically active particles by two studies. In the first study, we give a thorough discussion of the screening that occurs in Laplace problems. Three separate cases are considered: (1) Debye screening of a charged particle in an electrically neutral system, (2) Debye screening in a one component plasma (OCP) in which rapidly moving electrons screen the interactions between the slowly moving positive ions, and (3) systems in which the "charge" on a particle is proportional to the local potential, which results in so-called Brinkman screening. This last case is relevant for chemically active particles.

The second study applies the methodology to systems of chemically interacting phoretic particles where the system's evolution is tracked by simulations as formulated in Sec. III. In this study we show the onset of instability in a periodic domain when the phoretic velocity of particles is high and show that self-phoresis, as occurs for Janus particles, results in a more open cluster but cannot fully stabilize the system.

In a future study,[33] we discuss the stability of chemically active suspensions and show how the method developed in this paper can directly determine the stability boundary. In a related work,[34] we use the methodology developed here to study a finite 2D system in which active Janus particles are confined to a monolayer and constrained to lie within a circle of large radius. In this case we show how the distribution of particles can be predicted analytically via a coupled set of continuum-scale conservation equations for the suspensions stress, particle flux, and reactant concentration.

A. Screening in Laplace systems

Screening occurs in Laplace problems when the long-ranged $1/r$ interactions change over to an exponentially screened interaction $e^{-r/L_B}/r$, where the screening length L_B depends on the number density (or concentration) of "charged" particles. This only occurs in an "infinite" system; a finite number of charged particles does not (formally) exhibit screening. We first discuss the familiar Debye screening.

There are a number of ways to derive the Debye screening and the approach we take here allows us to discuss all three screening cases from the same perspective and so highlights their similarities and differences. We start from Hinch's averaged-equation method[35] to describe a dilute electrostatic system consisting of point charges q_α and a uniformly distributed charge density ρ (which is equivalent to $\langle s\rangle$). The ensemble average of any quantity is computed by multiplying by the N-particle configurational probability distribution function $P_N(\boldsymbol{X}_N)$ and integrating over particle positions $\boldsymbol{X}_N$. For a dilute system only the two-body conditional distribution function $P_{\beta|\alpha}$ is required, which gives the probability density for finding particle β relative to α (averaged over all possible configurations for the $N-2$ other particles). Particle α can be considered as fixed in space because only the relative configuration is relevant for a statistically homogeneous system. The ensemble averaged Laplace's equation becomes

$$\lambda\nabla^2\langle\varphi\rangle_\alpha(\boldsymbol{r}) = P_{\beta|\alpha}(\boldsymbol{r}_\beta-\boldsymbol{r}_\alpha)\langle q_\beta\rangle_\alpha + \langle\rho\rangle, \tag{35}$$

where λ stands for the permittivity ϵ for an electrostatic system and the solute diffusivity D_R for a reactive system, and φ denotes the electrostatic potential or the solute concentration. Finally, $\langle\,\rangle_\alpha$ denotes the conditional average with the α-particle fixed at $\boldsymbol{r}_\alpha$. Equation (35) applies outside the particle α.

1. Debye screening

Debye screening applies to a neutral electrolyte in which there are as many positive as negative charges and therefore $\langle\rho\rangle\equiv0$. Furthermore, the particle charges are fixed, which for simplicity, we take to be $\pm q$. In (35) we must distinguish separately the probability density for finding positive and negative charges outside the particle α (which itself could be either $\pm$) and thus (35) becomes

$$\lambda\nabla^2\langle\varphi\rangle_\alpha(\boldsymbol{r}) = \left[P_{+|\alpha}(\boldsymbol{r}_\beta-\boldsymbol{r}_\alpha) - P_{-|\alpha}(\boldsymbol{r}_\beta-\boldsymbol{r}_\alpha)\right]q. \tag{36}$$

The charged particles move freely and their distribution is governed by the competition between the electrostatic energy and the thermal energy k_BT. At equilibrium the Boltzmann distribution holds with $P_{+|\alpha}\sim n_+e^{-q\langle\varphi\rangle_\alpha/k_BT}$ and $P_{-|\alpha}\sim n_-e^{+q\langle\varphi\rangle_\alpha/k_BT}$, with $n_+=n_-=n$. Thus, the RHS of (36) becomes

$$\left[P_{+|\alpha}(\boldsymbol{r}_\beta-\boldsymbol{r}_\alpha) - P_{-|\alpha}(\boldsymbol{r}_\beta-\boldsymbol{r}_\alpha)\right]q \tag{37}$$

$$= nq\left[e^{-q\langle\varphi\rangle_\alpha/k_BT} - e^{+q\langle\varphi\rangle_\alpha/k_BT}\right]$$

$$= -2nq\sinh(q\langle\varphi\rangle_\alpha/k_BT), \tag{38}$$

which for small potentials gives

$$\nabla^2\langle\varphi\rangle_\alpha(\boldsymbol{r}) + \langle\varphi\rangle_\alpha/L_D^2 = 0, \tag{39}$$

with Debye screening length $L_D = (2nq^2/\epsilon k_B T)^{-1/2}$. The potential now behaves as $e^{-r/L_D}/r$ outside the particle α.

2. One component plasma (OCP)

A one component plasma typically consists of positive ions surrounded by an equal number of negative electrons. While the system is overall electrically neutral, the electrons move much more quickly than the positive ions and they form a background sea of uniform negative charge. The interest then is in the interaction between the positive ions and how their interaction is modified by the negative background. Equation (35) applies to this case, where now all particles α, β, etc., are the positively charged ions and the average charge density $\langle\rho\rangle = -n\langle q\rangle$ corresponds to the uniform sea of negative charge. Again, the ions are distributed according to the Boltzmann distribution and thus (35) becomes

$$\lambda\nabla^2\langle\varphi\rangle_\alpha(\boldsymbol{r}) = nq\,[e^{-q\langle\varphi\rangle_\alpha/k_BT} - 1], \tag{40}$$

where for simplicity we have taken all ions to have the same charge. For small potentials we have again Debye screening with the same screening length as we did for the neutral system.

In both of these systems, electrically neutral and the OCP, the screening is of a dynamic origin — the particles are Boltzmann distributed in response to the conditionally averaged potential. In the case of chemically active particles, a similar screening takes place, but it is static in origin and due to the fact that the "charge" of a reactive particle depends on the concentration field in which it finds itself.

3. Chemically active particles — Brinkman screening

The screening that takes place for chemically active particles will have the same exponential form as for Debye screening, but its origin is different. First, the screening is present even though the reactive particles can be uniformly distributed in space with a constant number density $P_{\beta|\alpha} = n$. For Debye screening it was essential that the probability for finding a second particle was given by the Boltzmann distribution with an energy that was proportional to the conditionally averaged potential $P_{\beta|\alpha} \sim e^{-\langle\varphi\rangle_\alpha/k_BT}$. For chemically active particles, the screening arises because the reaction rate $\langle r_\beta\rangle_\alpha$ (equivalent to the charge) is proportional to the local concentration. This screening is due to Brinkman who first showed the analogous screening for fluid flow through a dilute fixed bed of particles.[16]

Brinkman screening in reactive systems has been discussed in detail in Morris and Brady.[17] Here we briefly show how this comes about. We first rewrite (35) in terms of the concentration and reaction rate rather than potential and charge,

$$D_R\nabla^2\langle c\rangle_\alpha(\boldsymbol{r}) = P_{\beta|\alpha}(\boldsymbol{r}_\beta - \boldsymbol{r}_\alpha)\langle r_\beta\rangle_\alpha - \langle s\rangle. \tag{41}$$

If we average (41) over all positions of particle α, we have the unconditionally averaged equation — no particles fixed — for the average concentration field $\langle c\rangle$. Since $\nabla^2\langle c\rangle = 0$ in the statistically homogeneous suspension, the average of (41) shows that $n\langle r_\beta\rangle = \langle s\rangle$ — the average reaction rate is equal to the uniform average source of reactant. When particle β is far from particle α in (41), the conditionally averaged reaction rate must approach the bulk value, $\langle r_\beta\rangle_\alpha \to \langle r_\beta\rangle$, and thus, the RHS forcing in (41) is $n(\langle r_\beta\rangle_\alpha - \langle r_\beta\rangle)$, for a uniform distribution of particles β. For a first order surface chemical reaction (cf. (5)), the reaction rate is proportional to the concentration, and thus, to leading order in the number density of reactant particles (41) can be written as

$$D_R\nabla^2\langle c\rangle_\alpha(\boldsymbol{r}) = -na^2\kappa_0(\langle c\rangle_\alpha(\boldsymbol{r}) - \langle c\rangle). \tag{42}$$

The disturbance concentration $c' = \langle c\rangle_\alpha - \langle c\rangle$ is the relevant quantity and is screened: $c' \sim e^{-r/L_B}/r$, where as is the case for Debye screening, the Brinkman screening length is proportional to $n^{-1/2}$. Specifically, for uniformly reactive sink particles,

$$L_B^S/a = \sqrt{\frac{1+\mathrm{Da}}{3\phi\mathrm{Da}}}, \tag{43}$$

where the Damköhler number $\mathrm{Da} = \kappa_0 a/D_R$. For half-reactive Janus particles,

$$L_B^J/a = \sqrt{\frac{4\pi}{-3\phi f_c^q}}, \tag{44}$$

where f_c^q is the response function given in Appendix B. Here, $\phi = 4\pi a^3 n/3$ is the volume fraction of reactant particles. (A more complete derivation of L_B, with corrections for higher volume fractions and including many-body effects, can be found in the work of Morris and Brady.[17])

In the simulation method described in this work, we solve for the concentration field by summing all the long-ranged multipole interactions among particles. Therefore, that we recover Brinkman screening is a validation that our simulation method works properly. To test this, we generate a random but homogeneous configuration of N particles $(\boldsymbol{r}_1,\boldsymbol{r}_2,\ldots,\boldsymbol{r}_N)$ in a periodic box and solve for the particle multipoles with their positions fixed. Then one particle, denoted as particle 0, is randomly chosen and removed from the system, while the other particles are held fixed in space at their original positions. For the $N-1$ particles remaining after removal, their multipoles $(q_\beta,\boldsymbol{S}_\beta,\ldots)$ change. There is less competition for the reactant, and hence, the particle reactivity is higher: $q_{i,\mathrm{after}} < q_{i,\mathrm{before}} < 0$. We calculate the change in monopole strength $\Delta q_i = q_{i,\mathrm{before}} - q_{i,\mathrm{after}}$ of each (not removed) particle i and plot this against the distance of particle i from the removed particle 0. In the case of Janus particles, the orientation of each particle is randomly chosen and also fixed before and after removal.

When a particle is removed, the other particles feel the screened disturbance. According to Faxen laws (12) and (15), and screening lengths (43) and (44), q_i changes

according to

$$\text{For Sink: } \Delta q_i = -\frac{\text{Da}}{1+\text{Da}} q_0 e^{-r_{0,i}/L_B^S}/r_{0,i}, \tag{45}$$

$$\text{For Janus: } \Delta q_i = \frac{f_c^q}{4\pi} q_0 e^{-r_{0,i}/L_B^J}/r_{0,i}, \tag{46}$$

where $r_{0,i}$ is the distance between particles i and 0. The results are presented in Fig. 2 and clearly show Brinkman screening. Outside the Brinkman screening length, the particle monopole strength q_i hardly changes no matter whether particle 0 is in the system or not.

Our method thus resolves Brinkman screening properly, but before we proceed to the results for dynamic systems, it must be remarked that Brinkman screening arises only *after* the many-body concentration field $c(\boldsymbol{r})$ is computed properly. This means that one cannot simply prescribe a Yukawa-type interaction potential, $e^{-\alpha r}/r$, between the reactive particles and bypass the solution for the concentration field. By contrast, in an electrostatic system, pairwise Yukawa potentials can sometimes be applied when the counter-ions are much smaller and more mobile than the macro-ions, because under these conditions the fast counter-ions are subject to the Boltzmann distribution and are "dragged" along by the macro-ions to screen the electrostatic field between them. Therefore, the electrostatic system can be modeled as consisting of only macro-ions with pairwise Yukawa potentials to simplify the calculation of macro-ion motion. This is not possible for chemically active particles.

Moreover, a dynamic diffusiophoretic system is even more difficult to probe from the one-particle fixed average Equation (35) point of view. In a dynamic system, not only is q_α (or q_β) changing, but also the distribution $P_{\beta|\alpha}$ is altered by both diffusiophoresis and by Brownian motion (6). Although Brownian motion is thermal and by itself obeys the k_BT Boltzmann statistics, the Boltzmann distribution does not apply in general for $P_{\beta|\alpha}$. There is no Hamiltonian or interaction energy for the diffusiophoretic problem.

Finally, it should be appreciated that chemical screening is an essential aspect of diffusiophroretic suspensions. If there were no screening, then the diffusiophoretic attraction between particles would behave as $1/r^2$, which results in an unconditionally unstable system, leading to a collapse of all particles into a dense cluster, analogous to gravitational collapse. The fact that the chemical reactivity of a particle depends on the local concentration of fuel is the key to screening and to a possibly stable distribution of particles.

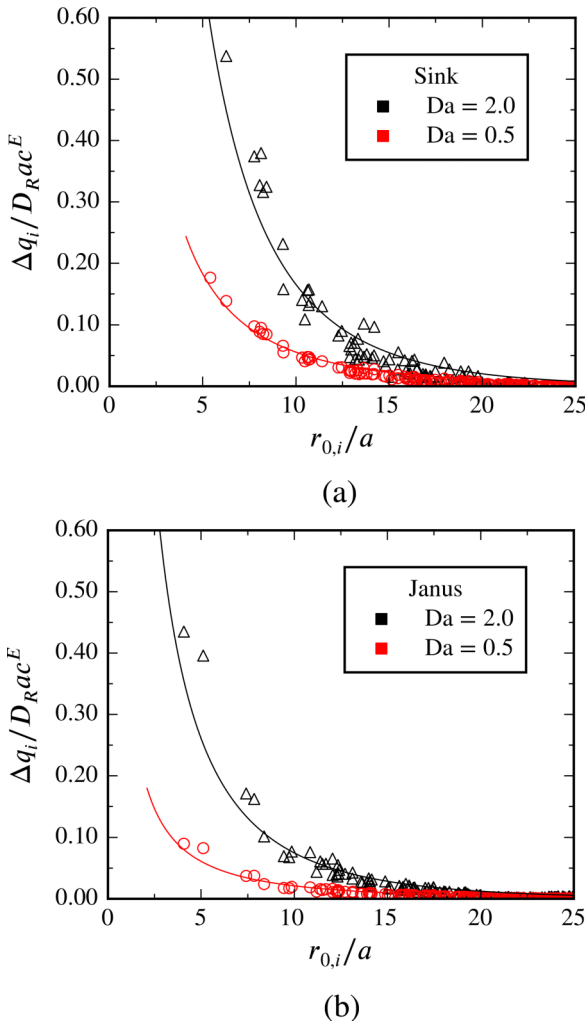

FIG. 2. Change of particle reactivity Δq_i in the vicinity of the removed test particle. Markers are simulation data and solid lines are the theoretical predictions for Brinkman screening (45). Simulation data are from a single configuration with $N = 625$, $\phi = 0.01$ (cubic periodic box $= 64 \times 64 \times 64 a^3$). Particles are randomly distributed.

B. Dynamic evolution of reactive particles

We first discuss the scalings for the diffusiophoretic system to introduce the important nondimensional parameters and the physically realistic parameter space to be explored. We choose the particle radius a as the length scale and the particle translational diffusion time a^2/D as the time scale, where $D = k_BT/6\pi\eta a$ is the reactive particle's translational diffusivity from the Stokes-Einstein-Sutherland relation. (Not to be confused with the solute reactant diffusivity $D_R \gg D$.) Reactant concentration (expressed as number density) is scaled by c^E, the externally imposed concentration: $c^E = c^\infty$ for the finite case and $c^E = \langle c \rangle$ for the periodic case, respectively. With these chosen scalings, the non-dimensional variables follow: particle velocity, $\hat{\boldsymbol{U}} = \boldsymbol{U}a/D$; concentration, $\hat{c} = c/c^E$; and multipoles: $\hat{q} = q/D_R a c^E$, $\hat{\boldsymbol{S}} = \boldsymbol{S}/D_R a^2 c^E$, and $\hat{\boldsymbol{Q}} = \boldsymbol{Q}/D_R a^3 c^E$. The nondimensional particle velocity due to the osmotic force from Equation (1) then becomes

$$\hat{\boldsymbol{U}} = -S_D \int_{\hat{S}} \hat{c}\, \boldsymbol{n}\, d\hat{S}, \tag{47}$$

where

$$S_D = (1 - \theta D_R/D_P)\, L(\Delta) c^E a^3, \tag{48}$$

which is the ratio of the speed due to phoresis $U^{ph} \sim L(\Delta) k_B T c^E a^2/6\pi\eta a$ to the characteristic velocity due to Brownian motion $U^B \sim D/a = k_BT/6\pi\eta a^2$. We shall refer to S_D as the "fuel strength;" it can also be thought of as a Peclet number: $U^{ph}a/D$. Recall that $(1 - \theta D_R/D_P)$ is the scaling factor for the reaction $R \to \theta P$, while $L(\Delta)$ measures hydrodynamic flow in the region of size $\Delta = \delta/a$ adjacent to the particle where the solute-particle interaction is operative. The imposed concentration c^E is taken to be constant in

time. Thus, for a given concentration level, stoichiometry, and interactive length, S_D is prescribed and fixed. The concentration field $\hat{c}$ is also dependent on the Damköhler number, $\mathrm{Da} = \kappa_0 a/D_R$, which thus indirectly affects a reactant particle's velocity.

The particle displacement from (6) in each time step is

$$\Delta\hat{\boldsymbol{X}} = \hat{\boldsymbol{U}}\Delta\hat{t} + \Delta\hat{\boldsymbol{X}}^B + \Delta\hat{\boldsymbol{X}}^{HS} = -S_D\hat{\boldsymbol{B}}\Delta\hat{t} + \Delta\hat{\boldsymbol{X}}^B + \Delta\hat{\boldsymbol{X}}^{HS}, \quad (49)$$

where $\hat{\boldsymbol{B}}_\alpha = \boldsymbol{B}_\alpha/a^2c^E$ from (16).

As discussed in Section II, for repulsive source particles $(1-\theta D_R/D_P) < 0$, while for attractive chemical sinks $(1-\theta D_R/D_P) > 0$. Therefore according to the definition of S_D in (48), for $S_D > 0$ we simulate the motion of attractive chemical sinks, while $S_D < 0$ corresponds to repulsive sources. If $S_D = 0$, there is no reaction-induced motion and the system degenerates to Brownian hard spheres as seen from (49).

In experiments the particles are typically micron-sized and $(1-\theta D_R/D_P) \sim O(1)$. In this work we consider the limit where solute or reactants are much smaller than the phoretic particles. For instance, in the experiments of Theurkauff *et al.*,[3] the solutes are hydrogen peroxide and oxygen molecules, both of which are at the nano-scale. In this limit $L(\Delta)a^3 \sim \delta^2 a$, where $\delta \sim O(10^{-9}$ m). Therefore $S_D \sim L(\Delta)a^3c^E \sim O(0.1)$ for $c^E \sim 1$ mMol/L $\sim 10^{23}/\mathrm{m}^3$ and $S_D \sim O(100)$ for $c^E \sim 1$ Mol/L. We shall focus on the fuel strength range, $0.1 < S_D < 10$, which appears to be sufficient to cover the important system behavior.

For negative $S_D < 0$, the diffusiophoretic particles repel each other and, when the repulsion is strong enough, a crystalline structure may be formed. Such diffusiophoretic repulsive "crystals" have been observed by Derjaguin and Goloovanov.[36] From the ensemble average equation perspective of (35), when repulsion is strong, $P_{\beta|\alpha}$ is "frozen" to a fixed point and q_α (and q_β) also approach constants. Therefore, the system becomes similar to an OCP. A detailed discussion of the crystallization behavior for repulsive diffusiophoretic particles will be reported elsewhere.

In an atomic or molecular system with short-range attractive interaction potentials, a gas-liquid phase transition can occur. For Active Brownian Particles (ABPs) a gas-liquid phase transition can also occur even though the interactions are repulsive (hard-sphere collisions). Each ABP propels itself at a given velocity $U_0\boldsymbol{\xi}$, and the direction $\boldsymbol{\xi}$ is subject to rotational Brownian motion. The translational random walk that results from the rotational Brownian motion generates a unique swim pressure,[12] analogous to the osmotic pressure of Brownian solutes. However, unlike the osmotic pressure, the swim pressure is a decreasing function of the active particle concentration, which can destabilize the system. Even though the ABPs are intrinsically non-equilibrium, a "thermodynamic"[13] description is possible with the active pressure providing an equation of state.

In chemically active particle systems, the long-range and non-pairwise additive nature of the phoretic interactions calls into question the notion of a "phase." We take up this question in a future work.[34]

In Secs. IV B 1 and IV B 2, we discuss the system dynamics via a particle-tracking simulation that solves the concentration field $c(\boldsymbol{r}; \boldsymbol{X}_N(t))$ at each and every time step and evolves the particle positions according to (49).

1. Attractive sink particles: Periodic systems

Attractive (non-Janus) sink particles show very interesting dynamics. In the limit of $S_D \to 0$, the system reduces to passive Brownian particles and remains a random but statistically homogeneous distribution of particles until the freezing density ($\phi \approx 0.5$). At the other extreme of high S_D, the fuel concentration is high and particle-particle attractions are strong and clusters are formed. In this section, we focus on the range of S_D where the long-time or steady-state structure transitions from homogeneous to clustering.

All simulations start from a random configuration of 2503 particles in a cubic unit cell of $64 \times 64 \times 64a^3$ with periodic boundary conditions. Results will be presented for a single volume fraction, $\phi = 0.04$, and a single Damköhler number, $\mathrm{Da} = 2.0$, but for S_D ranging from 0.3 to 6.0. The multipole moment expansion is truncated at the dipole level. For analysis purposes the particle reactivity q is compared to the isolated single particle reactivity from (12): $q_0 = -4\pi D_R a c^E \mathrm{Da}/(1+\mathrm{Da})$. The "reactivity" ratio, q/q_0, shows the effect of particle clustering as a particle in the center of a cluster must compete with its neighbors for the reactant and its reactivity decreases. The clustering behavior is also analyzed by defining a local volume fraction, ϕ_p, which is the ratio of particle volume $4\pi a^3/3$ to the voronoi cell volume V_{voro} formed by the particle with its surrounding neighbors.

Fig. 3 shows the average reactivity $\langle q\rangle/q_0$ as the system evolves in time. At $S_D = 0.3$, the average reactivity $\langle q\rangle/q_0$ is unchanged, showing only small fluctuations. Particles remain randomly distributed, and a snapshot at steady state (A) shows that each particle has almost the same reactivity q. The statistics of ϕ_p in Fig. 4 show a narrow distribution around the imposed global volume fraction $\phi = 0.04$. Here $\langle q\rangle/q_0 > 1$ because the average reactivity is increased by many-body effects as ϕ increases for a homogeneous infinite suspension. The dependence $\langle q\rangle \sim \phi$ is discussed in the work of Bonnecaze and Brady.[20]

When S_D is increased to 0.9, clusters are formed. The reactivity $\langle q\rangle/q_0$ gradually decays and almost reaches a steady state by $t = 300a^2/D$. The simulation was continued to $t = 700a^2/D$ to ensure that the system did reach a steady state. As seen in Fig. 3, local fluctuations in volume fraction first form (B1), and the cluster continues to grow until limited by reaction and the size of the periodic unit cell. At steady state (B2) all particles in the box form a single cluster. The particle reactivity is very low inside the cluster, although the ϕ_p measurement in Fig. 4 shows that the local density is not high, $\phi_p \approx 0.08$. Only a few particles near the cluster surface (the green ones) maintain a significant reactivity near q_0.

When S_D is increased further to 6.0, the system evolves very quickly. In a very short time, $t \approx 4a^2/D$, a transient

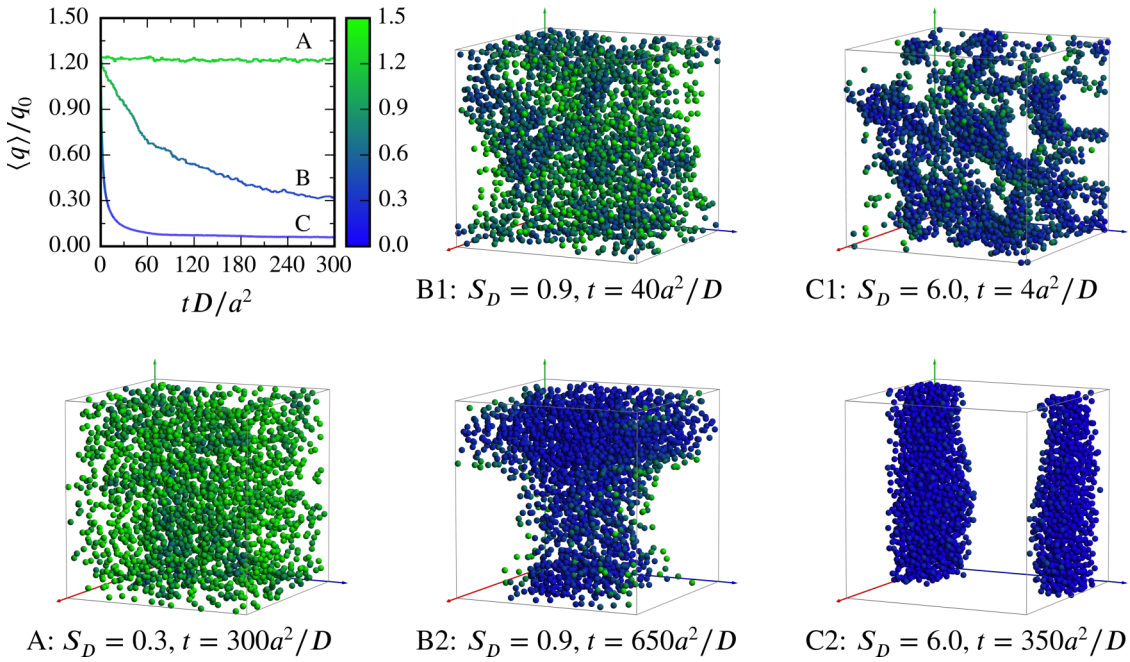

FIG. 3. Reactivity $\langle q\rangle/q_0$ of the sink system for different values of the fuel strength: (A) $S_D = 0.3$, (B) $S_D = 0.9$, and (C) $S_D = 6.0$ for $\phi = 0.04$, and Da = 2.0. There are $N = 2503$ particles in the cubic periodic unit cell. All cases start from a randomly distributed particle configuration. Particles are colored by reactivity $\langle q\rangle/q_0$. (A) is a system snapshot at steady state. (B1) and (C1) are snapshots in transient states, and (B2) and (C2) are at the steady states, respectively.

gel-like structure (C1) forms, and the average reactivity $\langle q\rangle/q_0$ reaches a very low level. Such a short evolution time means that the particles' diffusive motion, which is on the time scale a^2/D, has almost no effect on the initial evolving transient structure. The clustering process continues and reaches a steady state at about $t = 100a^2/D$. At steady state ($t = 300a^2/D$, C2), all particles collapse into a single cluster; there is no coexistence phenomena — no dilute single particles. The statistics of ϕ_p show that the local volume fraction is around 0.2, still very far from the close packing limit where $\phi > 0.5$. It is important to note that the peak close to $\phi_p = 0$ corresponds to those particles on the cluster surface, rather than a dilute phase, as is clear from C2 in Fig. 3.

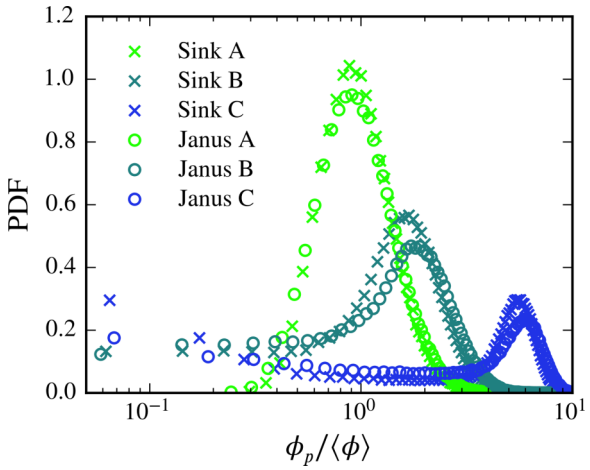

FIG. 4. Probability distribution of local particle volume fraction ϕ_p at the steady state. Here $\langle\phi\rangle = 0.04$, $N = 2503$, and the periodic box $= 64\times64\times64a^3$ for both sink and Janus particles. Da = 2.0 for sink and Da = 5.0 for Janus particles. The steady state configurations are A, B2, and C2 in Fig. 3 for sink particles and those in Fig. 5 (Multimedia view) for Janus particles.

2. *Attractive Janus particles: Periodic systems*

In this section we study the case of Janus particles that both self-propel and attract each other via diffusiophoretic interactions. Similar to the previous examples of sink systems, we simulate $N = 2503$ Janus particles in a periodic cubic unit cell of $64\times64\times64a^3$. All simulations start from a homogeneously random configuration and orientation distribution. Results are presented for a single volume fraction, $\phi = 0.04$, and a single Damköhler number, Da = 5.0, but for S_D ranging from 0.3 to 6.0. The multipole moment expansion is truncated at the dipole level for faster simulation. In most experimental realizations, the surface catalytic decomposition of H_2O_2 is very fast and Da $\approx O(10 \sim 1000)$.[37] Here, Da = 5.0 is chosen because the self-propulsion velocity reaches a plateau at around Da ≥ 5 due to the diffusion-limited nature of the chemical reaction.[14] The quantitative relation between Da and self-propulsion velocity is given by g_c^z in Appendix B. In contrast to the single-particle reactivity of a sink particle $q_0 = -4\pi D_R a c^E \mathrm{Da}/(1+\mathrm{Da})$, each Janus particle consumes $q_0^J = f_c^q D_R a c^E$, which also scales as $4\pi\mathrm{Da}/(1+\mathrm{Da})$ due to the reaction-diffusion nature but includes an extra factor to describe the Janus surface pattern. f_c^q is given in Appendix B. As in the previous case for sinks, q/q_0^J shows the effect of particle clustering because a particle in a crowded environment must compete with its neighbors for the reactant and its reactivity decreases.

Fig. 5 (Multimedia view) shows the system dynamics. Similar to the sink particles, when $S_D = 0.3$, the structure remains homogeneously distributed. When S_D is increased to 0.9, clusters form (B1). The reactivity $\langle q\rangle/q_0$ gradually

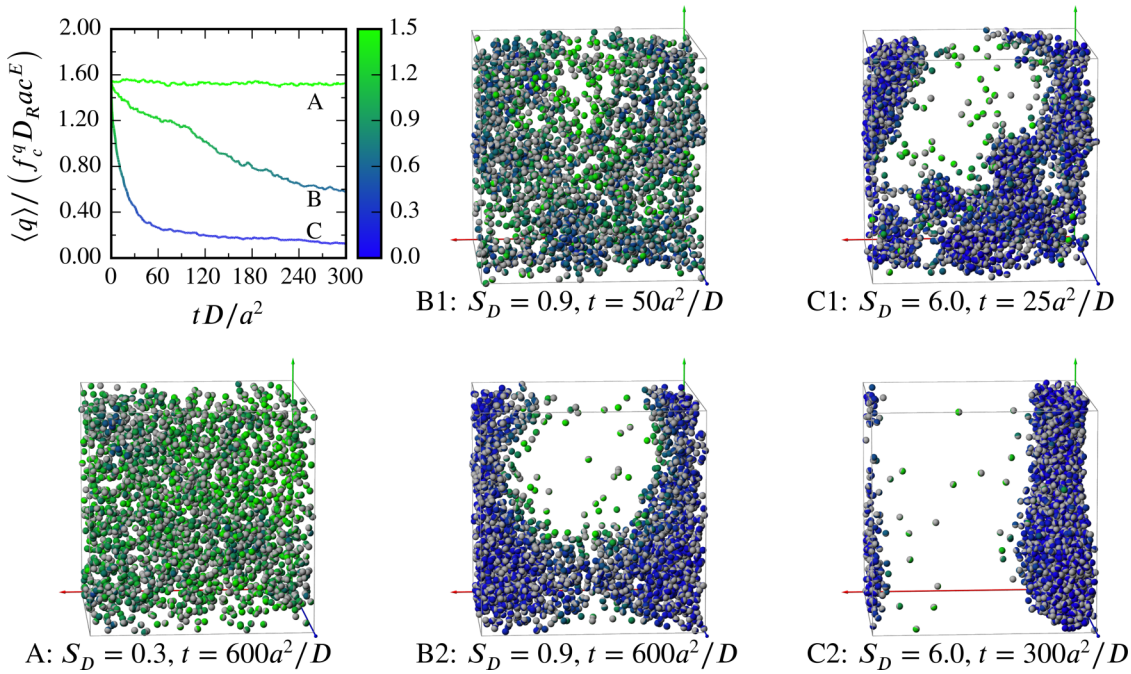

FIG. 5. Reactivity $\langle q\rangle/\left(f_c^q D_R a c^E\right) = q/q_0^J$ of the Janus systems for different values of the fuel strength: (A) $S_D = 0.3$, (B) $S_D = 0.9$, and (C) $S_D = 6.0$ for $\phi = 0.04$ and Da = 5.0. There are $N = 2503$ Janus particles in the cubic periodic unit cell. All cases start from a randomly distributed particle configuration, with uniform random orientation. The non-reactive hemispheres are colored gray, and the reactive hemispheres are colored by reactivity $\langle q\rangle/\left(f_c^q c^\infty\right)$, the consumption rate of reactant on each particle. The color map for q/q_0^J is the same as that in Fig. 3. (A) is a system snapshot at steady state. (B1) and (C1) are snapshots in transient states, and (B2) and (C2) are at the steady states, respectively. The movie illustrating the evolution of Case C is available as an integral multimedia file. (Multimedia view) [URL: http://dx.doi.org/10.1063/1.4963722.1]

decays and almost reaches a steady state by $t = 300a^2/D$. The simulation was continued to $t = 600a^2/D$ to ensure that a steady state (B2) was reached. When S_D is increased further to 6.0, the system evolves very quickly. In a short time, $t \approx 20a^2/D$, small clusters (C1) are formed, and the average reactivity $\langle q\rangle/q_0^J$ reaches a very low level. The clustering process continues and reaches a steady state at about $t = 100a^2/D$. At steady state ($t = 300a^2/D$, C2), a large cluster forms and extends to the size of the entire periodic box.

The key difference between sink (non-Janus) and Janus particles is that Janus particles have a chance to escape from a cluster via their self-propulsion and can thus form a gaseous region in coexistence with the clusters as seen in (b2) and (c2) of Fig. 5 (Multimedia view), similar to the coexistence observed in experiments.[3]

The statistics of the local volume fraction ϕ_p at steady state in Fig. 4 shows the structure in different systems. For $S_D = 0.3$, both the sink and Janus systems remain homogeneously distributed, and ϕ_p of each particle fluctuates around the average $\langle\phi\rangle = 0.04$. When $S_D = 0.9$ and $S_D = 6.0$, clusters are formed, and particles show different ϕ_p determined by their local environment. The particles in clusters occupy a crowded environment and show a peak at around $\phi_p \approx 0.08$ for $S_D = 0.9$ and $\phi_p \approx 0.2$ for $S_D = 6.0$. When particles fall into a cluster, their reactivity and accordingly attraction decrease, and the local structure is determined by the balance between attraction and translational Brownian motion. In the cases simulated here, S_D is not large enough for the attraction to tightly bind the particles to form crystals. It is estimated that $S_D \approx O(100)$ is necessary to increase the attraction to form crystals as observed in the experiments.[4] Janus and sink particles show similar ϕ_p in the clusters, which means that the attraction is similar despite the quantitative difference in the phoretic mobility matrix $\boldsymbol{M}_B$. Fewer particles are in the cluster in the Janus case, however, because some of them are in the gaseous region.

In addition to the particles inside the cluster, there are two other types of particles: those on the surface of the cluster and those in the gaseous region. The sink particles on the cluster surface each occupy a large voronoi cell because no gaseous particles exist adjacent to them, while the Janus particles on the cluster surface must share the space with the gaseous ones. Therefore, the sink particles in Case C have higher probability of having a very low $\phi_p \approx 0.1\langle\phi\rangle = 0.004$ than the Janus particles in Case C, as seen in Fig. 4. In principal, the gaseous particles may form another peak with $\phi_p \ll \langle\phi\rangle$, however, because in simulations of thousands of particles only about 20 particles are gaseous, the peak is very tiny, and the PDF of Janus particles in $0.2 < \phi_p/\langle\phi\rangle < 1$ is only slightly increased compared to the sink particles. The coexistence of cluster, surface, and gaseous particles in Janus systems is dynamic as observed in experiments.[3] Some particles with favorable orientations may leave the cluster surface by self-propulsion, while some gaseous particles may condense on the cluster.

Although the coexistence seen in simulations in Fig. 5 (Multimedia view) is similar to what is observed in experiment,[3,4] there is a key difference: in the experiments, a number of small clusters form and, over the duration of the observations, they do not necessarily merge into a single large cluster. By contrast, in our simulations, the clusters always

extend to the size of the simulation cell no matter how large the cell (how many particles are used), and this occurred for both the 3D systems shown here and other monolayer systems we tested. When a large cluster forms, it consumes reactant and acts like a large chemical sink, and there is a reactant flux proportional to the gradient $\boldsymbol{j}_R = -D_R \nabla c$ to "feed" the cluster. The non-zero ∇c attracts the free particles and small clusters to the large cluster by diffusiophoresis and the large cluster coarsens. A self-consistent model based on the mechanical balance between the swim pressure[12] and the swim force[38] is able to explain the coexistence behavior in our model systems, which we report it in a future work.[34] The apparently stable small clusters observed in the experiments suggest that other effects may play a role such as interactions with the boundary below the (monolayer of) particles, hydrodynamic effects between the particles, etc., so that the pure diffusiophoretic process governed by Laplace's equation may not be sufficient.

3. Discussion

In this work, we probed the dynamics of chemically active particles with the Accelerated Laplacian Dynamics (ALD) method. The fundamental assumption of our model is that each active particle disturbs and is also driven by the concentration field of reactant, which is governed by Laplace's equation $\nabla^2 c = 0$.

Such a field-driven clustering behavior is quite different from that which occurs in a pairwise short-ranged system, e.g., Lennard-Jones particles. In a Lennard-Jones system,[39,40] the potential is fixed so that once a cluster starts to form, the clustering process continues until the particle-particle separation reaches the repulsive range of the pairwise potential. In a reactive active particle system, however, the attraction, which is due to the reactivity, is neither prescribed nor fixed but is a solution to the many-particle Laplace equation. Hence, when clusters start to form particles get close to each other and, for not too small Da (fast reaction), the reactant concentration can be locally depleted in a cluster and an individual particle's reactivity can become small ($q_\alpha \sim 0$). Chemically active particles thus lose their attraction and the clustering process stops, leaving a loosely packed structure. Due to this depletion in fuel concentration for diffusion-limited (high Da) particles, at intermediate S_D the system may lose its stability and collapse into a cluster, but the cluster is loosely packed because the translational Brownian motion tends to drive the system toward a homogeneous state. The steady structure is always a balance between the translational Brownian motion and the diffusiophoretic attraction. The higher the S_D, the denser the cluster. Recall that S_D measures the fuel strength and is proportional to the reactant concentration $\langle c \rangle$.

The system behavior is also quite different from a classic first order gas-liquid phase transition where a dense phase coexists with a dilute phase. In the sink system no coexistence was observed for all cases studied, which were in the range $0.1 < \mathrm{Da} < 10$, $\phi < 10\%$, and $S_D < 10$. Compared to the experiments of Theurkauff *et al.*[3] which seem to show phase separation and coexistence, the key difference is that reactive sink particles cannot propel themselves; their motion is due to diffusiophoresis in the concentration gradient of the other particles. We repeated the simulation for Janus particles that undergo self-diffusiophoresis in 3D periodic systems and confirmed that self-propulsion is the vital component for coexistence of chemically active suspensions. However, in contrast to the small "droplets" in experiments, the clusters always extended to the entire periodic box at a steady state.

Our findings for reactive sink and Janus systems suggest that there is a threshold S_D^*, below which the system is stable, while for $S_D > S_D^*$ the system is unstable and collapses into a cluster, which eventually extends to encompass all particles. Note that if there were no chemical screening, then the system would be unconditionally unstable — there would be no stability threshold ($S_D^* = 0$). Linear stability analysis of a similar system can be found in Karpov and Oxtoby,[41] where they analyzed a system of "growing and decaying" particles and predicted the existence of a threshold. In a more recent work, Saha *et al.*[42] gave a linear stability analysis of chemically active particles with self-propulsion, phoretic response, and chemotaxis based on a Smoluchowski mean-field description and predicted that an instability threshold exists, which depends on the fuel concentration $\langle c \rangle$, the self-propulsion, Brownian motion, and the attraction due to diffusiophoresis. These predictions have not yet been verified by simulation or experiment. The simulation algorithm presented in this work would allow one to extract the detailed information of the clustering process in various geometries and test the theoretical predictions.

More importantly, because sink and Janus systems demonstrate a similar structural change with different S_D in Fig. 4, we speculate that the threshold S_D^* may be the same for both sink and Janus systems. We have also completed a detailed theoretical analysis and found that an instability does exist as predicted in the literature, and the threshold S_D^* is indeed independent of self-propulsion — the instability growth rate becomes positive when attraction overcomes translational Brownian diffusivity, which differs from the prediction of Saha *et al.*[42] In our theory self-propulsion quantitatively reduces the growth rate but has no impact on the threshold, because its effects appear at a higher order in wave number than the competition between diffusiophoretic attraction and Brownian diffusion. We also show that, by properly accounting for the flux of active particles in the presence of the solute concentration gradient,[13] a simple coarse-grained continuum mechanics theory predicts the instability very well. Our theory is verified by simulations conducted with the method described in this paper and will be presented in a future work.[33]

V. CONCLUSIONS

In this work an efficient computational method — Accelerated Laplacian Dynamics (ALD) — was introduced to explore the behavior of chemically active particles through dynamic simulation. The method is based on multipole expansions of Laplace's equation for the chemical

concentration field and has the flexibility to deal with both uniformly reactive and Janus particles. In fact, particles with more complicated reactive patterns can be easily simulated by using the appropriate functions f and g in the matrices $\boldsymbol{C}$ and $\boldsymbol{M}_B$, and these functions can be determined with the same BEM method used in Appendix B. The ALD method is also flexible to deal with different geometries, including periodic 3D and monolayer simulation cells, and finite 3D and monolayer systems. Further, our ALD method can be extended to systems adjacent to a flat solid boundary that is either non-penetrating or absorbs the reactant, which may be appropriate for some of the experiments;[3] one only needs to add the "reflected" multipoles due to the boundary as done in the familiar method of images in electrostatics.

The simulations presented in this paper utilized only one CPU and GPU, but they can be extended to use parallel machines with the help of distributed FFT and sparse matrix libraries. After the reactant field is determined, other operations are for each particle only and are independent from one another and so there is no extra barriers to parallelization. To further improve the method, the Ewald sum done with FFT may be improved with the fast multipole method to avoid the large amount of memory required by the FFT on a regular mesh. The multipole method may also be combined with the immersed boundary method[43] to provide the flexibility to accommodate domains of complex geometry.

Utilizing the ALD method, we clarified the notion of screening in chemically active systems. Chemical screening is a static self-screening that is fundamentally different from the more familiar Debye screening. The screening is such that the interactions decay exponentially rather than algebraically with distance. It is important to note that the screening results only *after* the correct full solution of Laplace's equation have been obtained; it cannot be prescribed *a priori* as has been done in some previous work.[18] Furthermore, this screening is fundamentally different from that employed in the Keller-Segel model in which the chemical solutes are assumed to be absorbed by the medium itself (the suspending fluid). Experimentally,[3] chemical solutes such as H_2O_2 and O_2 are not absorbed (or produced) by the medium; the chemical reactions at the particle surfaces create or destroy the solutes, and these reactions are proportional to the local surface concentration which gives rise to the chemical screening.

This chemical screening plays a fundamental role in providing the stability threshold S_D^*. Without screening the long-ranged interaction $c \sim q/r$ results in the collapse of all particles into a single cluster. Mathematically, such collapse in the absence of Brinkman screening corresponds to the finite time blow-up discussed in some variations of Keller-Segel model[44,45] and is also similar to the collapse in self-gravitating Brownian particles. The threshold S_D^* has been briefly discussed in the work of Saha *et al.*[42] and shall be discussed in detail in our stability analysis.[33]

With the ALD method for sink particles, we showed that the system is stable and remains random for small S_D but a single cluster forms at higher S_D. The particles compete for reactant and so when they get close to each other, their reactivities are reduced and thus the attraction diminishes. Thus, at intermediate S_D where the system loses stability and collapses to a cluster, the cluster itself is loosely packed. Importantly, no coexistence between the dense and dilute regions was observed for the sink system. We always observed a large cluster occupying the entire simulation box. When a cluster forms, it acts as a strong chemical sink and requires a flux of reactant. This reactant flux induces a concentration gradient, ∇c, and every particle (and/or other small clusters) is attracted to the large cluster by diffusiophoresis. The final state is a balance of translational Brownian motion and diffusiophoretic attraction.

For Janus particles, we observed similar behavior and structure as for the sink particles (see Fig. 4), with the notable exception that due to their self-propulsion, Janus particles at the surface of the cluster can escape the cluster, and thus, isolated swimming particles can be seen outside the cluster (see Fig. 5 (Multimedia view)), suggestive of the coexistence behavior observation in experiment.[3]

In this paper all reaction-induced motion arose from diffusiophoresis, whether it be self- or conventional down-gradient-diffusiophoresis; Eq. (1) applies for all cases. As a result a single parameter S_D determines the strength of the diffusiophoretic motion compared to the translational Brownian motion. The parameter S_D is equivalently the non-dimensional fuel concentration and the ratio of the velocity due to diffusiophoresis and the velocity of Brownian motion ($S_D \sim U^{ph}/U^B$) as explained after Eq. (48). Changing S_D thus affects the diffusiophoretic attraction *and* the self-propulsion in the same manner. However, it is possible that the self-propulsion, while still proportional to the local fuel concentration, is governed by a different scale factor. For example, the self-motion may result from self-electrophoresis rather than self-diffusiophoresis. In this situation, S_D would govern the magnitude of the down-gradient-induced motion, and another, independent parameter, say S_D^{el}, would govern the self-motion of the Janus particles. This would allow a richer phase structure as now diffusiophoretic attraction could be weak as compared to self-motion ($S_D < S_D^{el}$), but both still dependent on the local fuel concentration c as determined by ALD. Interestingly, we find that the stability is still determined by S_D regardless of the magnitude of the self-propulsion.[33]

In this paper, we focused on the most fundamental aspects of chemically active suspensions, but a number of extensions are possible. For example, under some conditions the reactive solutes may also exert a torque $\boldsymbol{L}$ on the particles, which can be easily implemented by an equation $\boldsymbol{L} \sim (c, \nabla c)$ similar to (30). (The analysis of Brady[15] leading to (1) can be generalized straightforwardly for the torque.) Some interesting results of dumbbell-shaped (sphere-dimer) active particles have also been discussed,[46] and in our algorithm two or more particles can be either rigidly or flexibly connected to create such swimmers (with some minor modifications of the Faxen Laws and a proper treatment of the binding force[47]). Non-spherical particles can also be simulated — the multipole strengths now also depend on the particle shape, and uniformly

reactive non-spherical particles have been predicted to self-propel.[24]

In this work, hydrodynamic interactions between particles have been ignored, only the isolated particle's Stokes drag coefficient and translational Brownian diffusivity enter. Since most solutes diffuse very fast compared to the particles, $D_R \gg D$, the fluid velocity field has no effect on the concentration field c. Hydrodynamic interactions among the particles can be important, however, and a way forward is to combine ALD for the concentration field with Accelerated Stokesian Dynamics (ASD)[22] for the hydrodynamics. As a first attempt, the boundary condition for the Stokes flow is still no-slip, and in this case, the Stokes flow and solutes transport are completely decoupled. All we need to do in this case is to replace the Stokes drag $6\pi\eta a$ in (1) by the full resistance matrix $\boldsymbol{R}_{FU}$. A more satisfactory approximation is that the boundary condition for the Stokes flow should be determined by the local concentration field c in the presence of a surface slip velocity at the particle surface.[15,23] In this case, the Stokes flow can be solved after the solution of the solute field c. This is one-way coupling and still solvable by the method of ASD, with some minor modifications due to the slip velocity on the lubrication corrections and the Faxen laws relating Stokes flow multipoles (force $\boldsymbol{F}$, torque $\boldsymbol{L}$, and stresslet $\boldsymbol{S}$) to the surrounding flow. At present the role of hydrodynamics in the clustering process and the steady state structure is not known. Hydrodynamic interactions increase the drag when clustering occurs and slow down both translational and rotational motions. A particle-tracking simulation is necessary to understand the system behavior and combining ALD and ASD a future area of research.

ACKNOWLEDGMENTS

Wen Yan thanks Mu Wang, Charles Slominski, and James Swan for the documents and discussions on Accelerated Stokesian Dynamics. This work is supported by NSF Grant No. CBET-1437570.

APPENDIX A: FAXEN LAWS FOR A HOMOGENEOUSLY REACTIVE PARTICLE

Consider uniform reaction everywhere on the particle surface, $h(\boldsymbol{n}) = 1$. With the first order reactive boundary condition (5) for $\boldsymbol{n}\cdot\boldsymbol{j}_R$, the multipoles of particle α become

$$q_\alpha = -\kappa_0 \int_S c dS, \tag{A1}$$

$$\boldsymbol{S}_\alpha = (D_R - \kappa_0 a)\int_S \boldsymbol{n} c dS, \tag{A2}$$

$$\boldsymbol{Q}_\alpha = \left(2aD_R - \kappa_0 a^2\right)\left(\int_S \boldsymbol{nn} c dS - \frac{1}{3}\int_S \boldsymbol{I} c dS\right). \tag{A3}$$

Thus, we need 3 surface integrals of c: $\int_S c dS$, $\int_S \boldsymbol{n} c dS$, and $\int_S \boldsymbol{nn} c dS$.

For any point $\boldsymbol{x}$ on the surface S of some particle α, the integral[19] that represents the solution to Laplace's equation can be written as

$$c(\boldsymbol{x}) - c'(\boldsymbol{x}) - c^E(\boldsymbol{x}) = \frac{1}{4\pi}\int_{S_y}\left(\boldsymbol{j}_R(\boldsymbol{y})\frac{1}{D_R|\boldsymbol{x}-\boldsymbol{y}|} + c(\boldsymbol{y})\frac{\boldsymbol{x}-\boldsymbol{y}}{|\boldsymbol{x}-\boldsymbol{y}|^3}\right)\cdot\boldsymbol{n}_y dS_y. \tag{A4}$$

Here c denotes the actual field value, c' and c^E refer to other particles' perturbation and the imposed external field, respectively, and $\boldsymbol{y}$ is a vector on the particle surface.

Take integral $\int_{S_x} dS$ of both sides. For the left side we have

$$\int_{S_x}\left[c(\boldsymbol{x}) - c'(\boldsymbol{x}) - c^E(\boldsymbol{x})\right] dS = \int_S c dS - 4\pi a^2 (c' + c^E)|_{\boldsymbol{r}_\alpha}, \tag{A5}$$

where $(c' + c^E)|_{\boldsymbol{r}_\alpha}$ means that the values of c' and c^E are evaluated at the center of particle α, $\boldsymbol{r}_\alpha$. The right side becomes a double integral over both $\boldsymbol{x}$ and $\boldsymbol{y}$ on the surface. By exchanging the order of integration, we have

$$\int_S c dS - 4\pi a^2 (c' + c^E)|_{\boldsymbol{r}_\alpha} = \frac{a}{D_R}\int_S \boldsymbol{j}_R\cdot\boldsymbol{n} dS = \frac{a}{D_R} q, \tag{A6}$$

from which we get the Faxen law (12) for monopole q. One can easily check that if we put only one particle in infinite field with condition c^∞, the Faxen laws gives $q = -[4\pi \mathrm{Da}/(1+\mathrm{Da})] D_R a c^\infty$, which is the consumption rate of reactant on the particle surface and coincides with solution given by traditional methods, e.g., separation of variables.

The $\boldsymbol{S}_\alpha$ and $\boldsymbol{Q}_\alpha$ relations can also be derived in the same way, but require some lengthy math. We shall not repeat the process here. Also, the factor $\mathrm{Da}/(1+\mathrm{Da})$ covers both reaction-limited and diffusion-limited cases. In the diffusion-limited case ($\mathrm{Da}\to\infty$), $\mathrm{Da}/(1+\mathrm{Da}) \to 1$ and (12) reduces to the relations given in the work of Bonnecaze and Brady.[19] In the reaction-limited case $\mathrm{Da}\to 0$ and therefore $\mathrm{Da}/(1+\mathrm{Da}) \to \mathrm{Da}$, so that $q_\alpha \propto \mathrm{Da}$.

APPENDIX B: FAXEN LAWS FOR A JANUS REACTIVE PARTICLE

For Janus particles, the Boundary Element Method (BEM hereafter) is used to calculate the Faxen laws matrix. We follow the standard BEM convention, and the problem of singularity on the boundary, which often occurs in BEM method, is appropriately handled.[48]

The numerical solution is conducted for a Janus particle with its orientation vector $\boldsymbol{\xi} = \hat{\boldsymbol{z}}$. Due to symmetry, $\boldsymbol{C}$ (truncated at dipole level) takes the following form:

$$\begin{pmatrix} q \\ S_x \\ S_y \\ S_z \end{pmatrix} = \begin{pmatrix} f_c^q & 0 & 0 & f_{cz}^q \\ 0 & f_{cx}^{sx} & 0 & 0 \\ 0 & 0 & f_{cy}^{sy} & 0 \\ f_c^{sz} & 0 & 0 & f_{cz}^{sz} \end{pmatrix}\begin{pmatrix} c \\ (\nabla c)_x \\ (\nabla c)_y \\ (\nabla c)_z \end{pmatrix}, \tag{B1}$$

where S_x, S_y, and S_z are components of vector $\boldsymbol{S}$. $(\nabla c)_x$, $(\nabla c)_y$, and $(\nabla c)_z$ are components of ∇c. The five response functions, $f_c^q, f_{cz}^q, f_{cx}^{sx}, f_c^{sz}, f_{cz}^{sz}$, are functions of Da only. The BEM solution is done for Da in the range $(0.01, 100.0)$, covering both

reaction-limited ($\mathrm{Da} \to 0$) and diffusion-limited ($\mathrm{Da} \to \infty$) cases. The reactivity f functions are fitted by an interpolation form to allow each f to be evaluated for arbitrary Da,

$$f_c^q = -\frac{4\pi \mathrm{Da}}{1+\mathrm{Da}} \frac{0.72\mathrm{Da}^2 + 1.98\mathrm{Da} + 1}{\mathrm{Da}^2 + 3.26\mathrm{Da} + 2}, \tag{B2}$$

$$f_{cz}^q = -\frac{4\pi \mathrm{Da}}{1+\mathrm{Da}} \frac{0.46\mathrm{Da}^2 + 0.36\mathrm{Da} + 0.38}{\mathrm{Da}^2 + 0.82\mathrm{Da} + 1}, \tag{B3}$$

$$f_{cx}^{sx} = -2\pi \frac{\mathrm{Da} - 2.76}{\mathrm{Da} + 2.76}, \tag{B4}$$

$$f_c^{sz} = -\frac{4\pi \mathrm{Da}}{1+\mathrm{Da}} \frac{0.46\mathrm{Da}^2 + 0.39\mathrm{Da} + 0.38}{\mathrm{Da}^2 + 0.87\mathrm{Da} + 1}, \tag{B5}$$

$$f_{cz}^{sz} = -2\pi \frac{\mathrm{Da} - 7.77}{4.50\mathrm{Da} + 7.70}. \tag{B6}$$

The typical error of these fitting functions is around 2%. Here, we do not pursue the absolute accuracy because our interest is in the correct scaling of the response and the correct features of propulsion and interaction.

For particles with $\boldsymbol{\xi} \neq \hat{\boldsymbol{z}}$, rotation can be applied to the matrices $\boldsymbol{C}$,

$$\boldsymbol{C} = \begin{pmatrix} f_c^q & f_{cz}^q \xi_x & f_{cz}^q \xi_2 & f_{cz}^q \xi_z \\ f_c^{sz} \xi_x & f_{cz}^{sz} \xi_x^2 + f_{cx}^{sx}(1-\xi_x^2) & (f_{cz}^{sz} - f_{cx}^{sx}) \xi_x \xi_y & (f_{cz}^{sz} - f_{cx}^{sx}) \xi_x \xi_z \\ f_c^{sz} \xi_y & (f_{cz}^{sz} - f_{cx}^{sx}) \xi_x \xi_y & f_{cz}^{sz} \xi_y^2 + f_{cx}^{sx}(1-\xi_y^2) & (f_{cz}^{sz} - f_{cx}^{sx}) \xi_x \xi_z \\ f_c^{sz} \xi_z & (f_{cz}^{sz} - f_{cx}^{sx}) \xi_x \xi_z & (f_{cz}^{sz} - f_{cx}^{sx}) \xi_x \xi_z & f_{cz}^{sz} \xi_z^2 + f_{cx}^{sx}(1-\xi_z^2) \end{pmatrix}. \tag{B7}$$

Similarly, $\boldsymbol{M_B}$ is calculated from the orientation $\boldsymbol{\xi}$ and the fitted functions g_c^z, g_{cz}^z, and g_{cx}^x,

$$\boldsymbol{M_B} = \begin{pmatrix} g_c^z \xi_x & g_{cz}^z \xi_x^2 + g_{cx}^x (1-\xi_x^2) & (g_{cz}^z - g_{cx}^x) \xi_x \xi_y & (g_{cz}^z - g_{cx}^x) \xi_x \xi_z \\ g_c^z \xi_y & (g_{cz}^z - g_{cx}^x) \xi_x \xi_y & g_{cz}^z \xi_y^2 + g_{cx}^x (1-\xi_y^2) & (g_{cz}^z - g_{cx}^x) \xi_x \xi_z \\ g_c^z \xi_z & (g_{cz}^z - g_{cx}^x) \xi_x \xi_z & (g_{cz}^z - g_{cx}^x) \xi_x \xi_z & g_{cz}^z \xi_z^2 + g_{cx}^x (1-\xi_z^2) \end{pmatrix}, \tag{B8}$$

where

$$g_{cx}^x = 2\pi \frac{0.36\mathrm{Da}^2 + 2.55\mathrm{Da} + 1}{\mathrm{Da}^2 + 2.65\mathrm{Da} + 1}, \tag{B9}$$

$$g_c^z = -\frac{4\pi \mathrm{Da}}{1+\mathrm{Da}} \frac{0.16\mathrm{Da}^2 + 0.094\mathrm{Da} + 0.13}{\mathrm{Da}^2 + 0.60\mathrm{Da} + 1}, \tag{B10}$$

$$g_{cz}^z = 4\pi \frac{0.30\mathrm{Da}^2 + 0.95\mathrm{Da} + 0.5}{\mathrm{Da}^2 + 2.05\mathrm{Da} + 1}. \tag{B11}$$

APPENDIX C: ALL CONTRIBUTIONS OF $\mathcal{E}$ IN THE EWALD SUM

For compactness of the equations, we define

$$f(r) = \frac{\mathrm{Erfc}\left(\sqrt{\pi/\zeta} r\right)}{r}, \tag{C1}$$

and $\boldsymbol{r} = \boldsymbol{x} - \boldsymbol{y}$. Suppose that $\boldsymbol{x}$ is at the location of particle 1, $\boldsymbol{x} = \boldsymbol{y}_1$. In the summation, $\boldsymbol{y}_{other}$ means all other particles in space. $\boldsymbol{r} = \boldsymbol{x} - \boldsymbol{y}_\beta = \boldsymbol{y}_1 - \boldsymbol{y}_\beta$, and β denotes the other particles. In this context, $\nabla = \nabla_1 = \partial/\partial \boldsymbol{y}_1$, $\nabla_2 = \nabla_\beta = \partial/\partial \boldsymbol{y}_\beta$. The realspace sum, wavespace sum, and the self-correction terms are

$$\begin{aligned} c(\boldsymbol{y}_1) = \langle c \rangle &+ \frac{1}{4\pi D_R} \sum_{\beta \neq 1} \left(q_\beta^{eff} - \boldsymbol{S}_\beta \cdot \nabla_1 + \frac{1}{2} \boldsymbol{Q}_\beta : \nabla_1^{(2)} \right) f(r) \\ &+ \frac{1}{4\pi D_R V_0} \sum_{\boldsymbol{k} \neq 0} \sum_\beta \left(q_\beta^{eff} - \boldsymbol{S}_\beta \cdot \nabla_1 + \frac{1}{2} \boldsymbol{Q}_\beta : \nabla_1^{(2)} \right) e^{2\pi i \boldsymbol{k} \cdot (\boldsymbol{y}_\beta - \boldsymbol{y}_1)} \frac{e^{-\zeta \pi k^2}}{\pi k^2} \\ &+ \left(-\frac{1}{2\pi D_R \sqrt{\zeta}} \right) q_1^{eff} + \frac{1}{6 D_R \zeta^{3/2}} \mathrm{Tr} \boldsymbol{Q}_1, \end{aligned} \tag{C2}$$

$$\begin{aligned} \nabla c(\boldsymbol{y}_1) = &\frac{1}{4\pi D_R} \sum_{\beta \neq 1} \left(q_\beta^{eff} \nabla_1 - \boldsymbol{S}_\beta \cdot \nabla_1^{(2)} + \frac{1}{2} \boldsymbol{Q}_\beta : \nabla_1^{(3)} \right) f(r) \\ &+ \frac{1}{4\pi D_R V_0} \sum_{\boldsymbol{k} \neq 0} \sum_\beta \left(q_\beta^{eff} \nabla_1 - \boldsymbol{S}_\beta \cdot \nabla_1^{(2)} + \frac{1}{2} \boldsymbol{Q}_\beta : \nabla_1^{(3)} \right) e^{2\pi i \boldsymbol{k} \cdot (\boldsymbol{y}_\beta - \boldsymbol{y}_1)} \frac{e^{-\zeta \pi k^2}}{\pi k^2} + \left(-\frac{1}{3 D_R \zeta^{3/2}} \right) \boldsymbol{S}_1, \end{aligned} \tag{C3}$$

$$\text{and } \nabla\nabla c(\boldsymbol{y}_1) = \frac{1}{4\pi D_R}\sum_{\beta\neq 1}\left(q_\beta^{eff}\nabla_1^{(2)} - \boldsymbol{S}_\beta\cdot\nabla_1^{(3)} + \frac{1}{2}\boldsymbol{Q}_\beta\colon\nabla_1^{(4)}\right) f(r)$$
$$+ \frac{1}{4\pi D_R V_0}\sum_{\boldsymbol{k}\neq 0}\sum_{\beta}\left(q_\beta^{eff}\nabla_1^{(2)} - \boldsymbol{S}_\beta\cdot\nabla_1^{(3)} + \frac{1}{2}\boldsymbol{Q}_\beta\colon\nabla_1^{(4)}\right) e^{2\pi i\boldsymbol{k}\cdot(\boldsymbol{y}_\beta-\boldsymbol{y}_1)}\frac{e^{-\zeta\pi k^2}}{\pi k^2}$$
$$+ \left(\frac{1}{3D_R\zeta^{3/2}}\boldsymbol{I}q_1^{eff}\right) + \left(-\frac{\pi}{5D_R\zeta^{5/2}}\right)\boldsymbol{T}\colon\boldsymbol{Q}_1. \tag{C4}$$

Here $\nabla^{(i)}$ means to take ∇ operator i times, which gives the correct tensor structure. Tr is the trace operator, and $\boldsymbol{T}$ is the 4th order isotropic tensor: $\boldsymbol{T}_{ijkl} = (\delta_{ij}\delta_{kl} + \delta_{ik}\delta_{jl} + \delta_{il}\delta_{jk})$.

[1]S. Ebbens, R. A. L. Jones, A. J. Ryan, R. Golestanian, and J. R. Howse, Phys. Rev. E **82**, 015304 (2010).
[2]J. R. Howse, R. A. Jones, A. J. Ryan, T. Gough, R. Vafabakhsh, and R. Golestanian, Phys. Rev. Lett. **99**, 048102 (2007).
[3]I. Theurkauff, C. Cottin-Bizonne, J. Palacci, C. Ybert, and L. Bocquet, Phys. Rev. Lett. **108**, 268303 (2012).
[4]J. Palacci, S. Sacanna, A. P. Steinberg, D. J. Pine, and P. M. Chaikin, Science **339**, 936 (2013).
[5]S. Soh, K. J. M. Bishop, and B. A. Grzybowski, J. Phys. Chem. B **112**, 10848 (2008).
[6]A. P. Solon, J. Stenhammar, R. Wittkowski, M. Kardar, Y. Kafri, M. E. Cates, and J. Tailleur, Phys. Rev. Lett. **114**, 198301 (2015).
[7]G. S. Redner, A. Baskaran, and M. F. Hagan, Phys. Rev. E **88**, 012305 (2013).
[8]R. Wittkowski, A. Tiribocchi, J. Stenhammar, R. J. Allen, D. Marenduzzo, and M. E. Cates, Nat. Commun. **5**, 4351 (2014).
[9]A. M. Menzel and H. Löwen, Phys. Rev. Lett. **110**, 055702 (2013).
[10]J. Stenhammar, A. Tiribocchi, R. J. Allen, D. Marenduzzo, and M. E. Cates, Phys. Rev. Lett. **111**, 145702 (2013).
[11]M. E. Cates and J. Tailleur, Annu. Rev. Condens. Matter Phys. **6**, 219 (2015).
[12]S. C. Takatori, W. Yan, and J. F. Brady, Phys. Rev. Lett. **113**, 028103 (2014).
[13]S. C. Takatori and J. F. Brady, Phys. Rev. E **91**, 032117 (2015).
[14]U. M. Córdova-Figueroa and J. F. Brady, Phys. Rev. Lett. **100**, 158303 (2008).
[15]J. F. Brady, J. Fluid Mech. **667**, 216 (2011).
[16]H. C. Brinkman, Appl. Sci. Res. **1**, 27 (1949).
[17]J. F. Morris and J. F. Brady, Ind. Eng. Chem. Res. **34**, 3514 (1995).
[18]O. Pohl and H. Stark, Phys. Rev. Lett. **112**, 238303 (2014).
[19]R. T. Bonnecaze and J. F. Brady, Proc. R. Soc. A **430**, 285 (1990).
[20]R. T. Bonnecaze and J. F. Brady, J. Chem. Phys. **94**, 537 (1991).
[21]R. T. Bonnecaze and J. F. Brady, Proc. R. Soc. A **432**, 445 (1991).
[22]A. Sierou and J. F. Brady, J. Fluid Mech. **448**, 115 (2001).
[23]J. L. Anderson, Annu. Rev. Fluid Mech. **21**, 61 (1989).
[24]S. Shklyaev, J. F. Brady, and U. M. Córdova-Figueroa, J. Fluid Mech. **748**, 2488 (2014).
[25]D. R. Foss and J. F. Brady, J. Rheol. **44**, 629 (2000).
[26]D. M. Heyes and J. R. Melrose, J. Non-Newtonian Fluid Mech. **46**, 1 (1993).
[27]D. A. Beard and T. Schlick, Biophys. J. **85**, 2973 (2003).
[28]R. W. O'Brien, J. Fluid Mech. **91**, 17 (1979).
[29]A. Y. Toukmaji and J. A. Board, Comput. Phys. Commun. **95**, 73 (1996).
[30]T. Darden, D. York, and L. Pedersen, J. Chem. Phys. **98**, 10089 (1993).
[31]H. Nguyen, *GPU Gems 3* (Addison-Wesley Professional, 2007).
[32]M. Deserno and C. Holm, J. Chem. Phys. **109**, 7678 (1998).
[33]W. Yan and J. F. Brady, "Stability analysis of the clustering in chemically active particles: From continuum mechanics to detailed dynamics" (unpublished).
[34]W. Yan and J. F. Brady, "The dense-dilute coexistence of chemically active particles: A continuum mechanics perspective" (unpublished).
[35]E. J. Hinch, J. Fluid Mech. **83**, 695 (1977).
[36]B. Derjaguin and M. Golovanov, Colloids Surf. **10**, 77 (1984).
[37]S. Ebbens, M.-H. Tu, J. R. Howse, and R. Golestanian, Phys. Rev. E **85**, 020401 (2012).
[38]W. Yan and J. F. Brady, Soft Matter **11**, 6235 (2015).
[39]P. H. S. Santos, O. H. Campanella, and M. A. Carignano, J. Phys. Chem. B **114**, 13052 (2010).
[40]J. F. M. Lodge and D. M. Heyes, J. Chem. Phys. **109**, 7567 (1998).
[41]V. G. Karpov and D. W. Oxtoby, Phys. Rev. E **55**, 7253 (1997).
[42]S. Saha, R. Golestanian, and S. Ramaswamy, Phys. Rev. E **89**, 062316 (2014).
[43]A. P. S. Bhalla, B. E. Griffith, N. A. Patankar, and A. Donev, J. Chem. Phys. **139**, 214112 (2013).
[44]D. Horstmann, Nodea-Nonlinear Differ. **8**, 399 (2001).
[45]D. Horstmann and M. Winkler, J. Differ. Equations **215**, 52 (2005).
[46]S. Thakur and R. Kapral, Phys. Rev. E **85**, 26121 (2012).
[47]J. W. Swan, J. F. Brady, R. S. Moore, and ChE. 174, Phys. Fluids **23**, 71901 (2011).
[48]C. Pozrikidis, *A Practical Guide to Boundary Element Methods with the Software Library BEMLIB* (CRC Press, 2002).